RICE UNIVERSITY

GEORGE R. BROWN SCHOOL OF ENGINEERING

CAPABILITY OF ARRAY PROCESSING ALGORITHMS TO ESTIMATE SOURCE BEARINGS

Stuart R. De Graaf
Don H. Johnson

Department of Electrical Engineering
Rice University
Houston, Texas 77251

Technical Report #8218
December 1982

DEPARTMENT OF ELECTRICAL ENGINEERING

HOUSTON, TEXAS

CAPABILITY OF ARRAY PROCESSING ALGORITHMS TO ESTIMATE SOURCE BEARINGS

Stuart R. De Graaf
Don H. Johnson

Department of Electrical Engineering
Rice University
Houston, Texas 77251

Technical Report #8218
December 1982

This research was supported by the Office of Naval Research under Grant No. N00014-81-K-0565.

Capability of Array Processing Algorithms to Estimate Source Bearings

by

Stuart R. De Graaf*
Don H. Johnson

Department of Electrical Engineering
Rice University
Houston, Texas

Abstract

The capabilities of classical, minimum energy, and linear predictive array processing algorithms to estimate the bearings of two equal-energy sources is examined. Signal coherence is shown to affect adversely the resolution and detection capabilities, as well as the bias characteristics, of all three algorithms. For linear arrays of equally-spaced sensors, the superior resolution capability of the linear predictive algorithm is demonstrated. The value of utilizing prediction elements in the center of the array to resolve very closely-spaced source bearings is demonstrated. However, the linear predictive algorithm is least capable of detecting highly coherent sources. A tradeoff is established between resolving capability and sensitivity to finite averaging. Conditions are established which indicate which algorithm is best suited to anticipated levels of signal coherence and averaging. The estimates of source bearing produced by each algorithm are shown to be asymptotically biased. The bias produced by the classical beamformer is most severe, while the minimum energy beamformer produces the least bias.

1. Introduction

The determination of the bearings of distant sources of acoustic energy in a noisy ocean environment is a primary objective of a passive sonar system. A group of acoustic sensors arranged in a known spatial pattern (an array) is deployed to record the acoustic field. Classical or Bartlett beamforming, minimum energy (ME) adaptive beamforming[1], and linear predictive (LP) processing algorithms are commonly employed to estimate source bearings from array data [2]. These processing procedures result in **beam-patterns**, plots of estimated incident energy versus bearing-of-look (see figure 1).

Three criteria are used to evaluate the performance of a processing algorithm with respect to source bearing estimation. The first is **resolution**. When a single propagating plane wave impinges on the array, a global maximum occurs **on-target**, i.e., at the bearing of incidence. When two plane waves are incident, their presence may or not be evident in the beam-patterns. If separated in bearing by a sufficient amount, their bearings will be resolved, in which case the beam-patterns exhibit two distinct maxima as in figure 1. On the other hand, the beam-patterns may fail to resolve the source bearings; in this case, the beam-patterns display a single broad maximum located at some intermediate bearing. The beam-patterns corresponding to two unresolved sources can greatly resemble those

*This research was supported by Office of Naval Research Contract N00014-81-K-0565.

[1] This beamforming algorithm, due to Capon [1], is often referred to as the maximum likelihood method in the literature. Actually, the beam does not maximize a likelihood function; thus the customary terminology is misleading.

corresponding to a single source. Resolution analysis assesses the conditions under which an array processing algorithm is capable of resolving source bearings. A useful measure of the resolution capability of an array processing algorithm is the signal-to-noise ratio it requires to resolve two closely-spaced, equal-energy sources.

The beam-patterns produced by the processing algorithms exhibit small local maxima off-target (figure 1). These off-target ripples are referred to as **sidelobes**. The second criterion is the degree to which the sidelobes are small, so that they are not confused with peaks corresponding to incident energy. Thus, **detection analysis** assesses the conditions under which the number of targets present in the acoustic field can be determined accurately.

Finally, a processing algorithm can both detect and resolve sources but yield inaccurate estimates of the bearing of each target. **Bias analysis** assesses how much the estimates of source bearing deviate from the true target bearings.

Cox [3] analyzed the capability of the Bartlett and ME array processing algorithms to resolve two equal-energy, temporally uncorrelated, sources. He demonstrated that the ME algorithm can resolve closely-spaced source bearings at a lower signal-to-noise ratio than can the Bartlett algorithm. Studying the single source case, Seligson [4] observed that the performance of the ME algorithm is quite sensitive to deviations of the signal wavefront from its assumed planar shape. For example, the superposition of temporally correlated plane waves, which occurs in multipath environments, produces a net wavefront which is not planar. As multipath propagation is prevalent in the ocean [5], there is a need to understand how source correlation affects the resolving capabilities of array processing algorithms. This paper pursues an analysis similar to that of Cox to study the capabilities of Bartlett, ME, and LP algorithms to detect and resolve coherent (i.e. correlated, narrowband) signals using linear arrays of equally-spaced sensors (LES arrays). Furthermore, bias of the bearing estimates produced by the three algorithms is studied.

Our detection/resolution and bias analyses are based on the assumption that an infinite amount of ergodic array data is available, thereby allowing the cross spectral correlation matrix to be determined exactly by averaging over an infinite period of time. Consequently, these results are not sufficient to assess the performance capability of an algorithm used in practical situations. To provide some insight into the utility of each processing algorithm, guidelines are established which indicate the amount of averaging necessary to suppress variability of the beam-patterns due to finite averaging.

2. Signal Model

The acoustic field present in an ocean environment can be modelled as a finite superposition of P signal plane waves propagating with different bearings $\underline{k}_p$ and energies added to a background noise field having zero mean. Assuming that the m^{th} sensor is located at position $\underline{z}_m$, its output, sampled with period T, is

$$x_m(nT) = n_m(nT) + \sum_{p=1}^{P} s_p(nT - \frac{1}{c}\underline{k}_p \cdot \underline{z}_m) \qquad m = 0,1,2,\ldots,M-1 \qquad (1a)$$

M is the number of sensors in the array, c is the speed of propagation, and $\underline{k}$ is a dimensionless unit vector pointing along the bearing of propagation. We restrict our attention to array geometries which exhibit symmetry through the origin, i.e. $\underline{z}_{M-1-m} = -\underline{z}_m$, as in figure 2. By definition, the signals seen at the origin of the array

have zero delay. Such a model is said to be phase centered. Evaluating the discrete Fourier transform of (1a) yields

$$\underline{X}(f) = \sigma_0(f)\underline{N}(f) + \sum_{p=1}^{P} \Psi_p(f)\underline{S}_p(f). \tag{1b}$$

where each component in the complex M-dimensional vectors corresponds to an array element. $\sigma_0(f)\underline{N}(f)$ is the vector of discrete Fourier transforms of the noise, $\underline{S}_p(f)$ is the direction vector corresponding to source p with components $S_{pm} = \exp(-j2\pi \frac{f}{c} \underline{k}_p \cdot \underline{z}_m)$, and $\Psi_p(f)$ is the discrete Fourier transform of $s_p(nT)$. $\sigma_0^2(f)$ is the variance of the noise at frequency f and $\underline{N}(f)$ is normalized so that $E(\underline{N}'\underline{N}) = M$.

The following simple narrowband model is used to describe the signals:

$$s_p(nT) = \bar{\sigma}_p \, e^{j(2\pi f_p nT + \phi_p)}$$

where $\bar{\sigma}_p$ is a real deterministic amplitude constant, f_p is the deterministic center frequency, and ϕ_p is a random phase variable. The signal DFTs, evaluated at the analysis frequency f, are

$$\Psi_p(f) = \sigma_p \, e^{j\left[\phi_p + \pi(f_p - f)T(N-1)\right]}$$

where

$$\sigma_p = \bar{\sigma}_p \frac{\sin(\pi(f_p - f)TN)}{\sin(\pi(f_p - f)T)}. \tag{2}$$

Referring to figure 2, the components of the source direction vectors can be written as $S_{pm} = \exp(j\alpha_{p,m})$. Array geometry determines the parameters

$$\alpha_{p,m} = -2\pi \frac{f}{c} \underline{k}_p \cdot \underline{z}_m = -\frac{\pi r_m}{\lambda/2} \cos(\gamma_m - \theta_p),$$

where r_m and γ_m are the polar coordinates of the m^{th} sensor and θ_p is the bearing of the p^{th} source. λ is the common wavelength of the narrowband signals.

Each processing algorithm involves the evaluation of a functional[2]:

---

[2] For notational convenience, the dependence of the beam energies on frequency is

$$P_{BART}(\underline{k}) = \underline{W}'\underline{R}\underline{W} \tag{3a}$$

$$P_{ME}(\underline{k}) = \left[\underline{W}'\underline{R}^{-1}\underline{W}\right]^{-1} \tag{3b}$$

$$P_{LP_q}(\underline{k}) = \left|\underline{U}_q'\underline{R}^{-1}\underline{W}\right|^{-1}. \tag{3c}$$

R is the cross spectral correlation matrix [2]. $\underline{W}$ is the direction-of-look vector with elements $W_m = \exp(ja_m)$ where $a_m = -j2\pi \frac{f}{c}\underline{k}\cdot\underline{z}_m$, and $\underline{k}$ is the bearing-of-look. $\underline{U}_q$ is the prediction element vector containing a one in the q^{th} element and zeros elsewhere. The usual value of q for a LES array is 0, i.e. the prediction element is at the end of the array; here we consider the variation of using other prediction elements. Typically, a power of -2 rather than -1 is used for the LP algorithm. Here, use of the -1 power ensures that the units of (3a,b,c) agree and allows direct comparison of the resolving capabilities of the algorithms [2]. An equivalent formula for the LP beam energy which is more convenient for our analyses is

$$P_{LP_q}(\underline{k}) = \left[\underline{W}'\underline{B}_q^{-1}\underline{W}\right]^{-1/2} \tag{3d}$$

where $\underline{B}_q^{-1} = \underline{R}^{-1}\underline{U}_q\underline{U}_q'\underline{R}^{-1}$.

The foundation upon which this theoretical study rests is the assumed form of the cross spectral correlation matrix.

$$\underline{R} = E\left[\underline{X}\underline{X}'\right]$$

Using equation (1b), one obtains

$$\underline{R} = \sigma_0^2 E\left[\underline{N}\underline{N}'\right] + \sum_{p=1}^{P}\sigma_0\left[\underline{S}_p E\left[\Psi_p \underline{N}'\right] + E\left[\Psi_p^* \underline{N}\right]\underline{S}_p'\right] + \sum_{p=1}^{P}\sum_{m=1}^{P} E\left[\Psi_p \Psi_m^*\right]\underline{S}_p\underline{S}_m'.$$

The cross correlations of the signal DFTs are

---

suppressed. We examine the resolution and detection capabilities at a single analysis frequency.

$$E\left[\Psi_p \Psi_m^*\right] = \sigma_p \sigma_m E\left[e^{j(\phi_p - \phi_m)}\right] e^{j\pi(f_p - f_m)T(N-1)}.$$

The signal coherence coefficients are defined to be the normalized cross correlations

$$C_{pm} \equiv \frac{E\left[\Psi_p \Psi_m^*\right]}{\sigma_p \sigma_m} \tag{4}$$

and are analogous to correlation coefficients. It is easily shown that the magnitude of each coherence coefficient lies between zero and one. Furthermore, $C_{pm} = C_{mp}^*$. When signals p and m differ by only a constant deterministic phase and amplitude, they are perfectly coherent, i.e. $|C_{pm}| = 1$. This situation can arise, for example, when multiple propagation paths (with fixed differences in path length) exist between a single source and the array.

We consider the case where the noise is spatially white, has zero mean, and is independent of the signals. Subject to these assumptions, the cross spectral correlation matrix can be written as

$$\mathbf{R} = \sigma_0^2 \mathbf{I} + \mathbf{S}\mathbf{C}\mathbf{S}' \tag{5}$$

where the PxP coherence matrix C is composed of elements C_{pm}; S is an MxP matrix whose p^{th} column is $\sigma_p S_p$. Using a well-known matrix inverse formula [6], the correlation matrix inverse can be expressed as

$$\mathbf{R}^{-1} = \frac{1}{\sigma_0^2}\left[\mathbf{I} - \frac{1}{\sigma_0^2}\mathbf{S}\left[\mathbf{I} + \frac{\mathbf{C}\mathbf{S}'\mathbf{S}}{\sigma_0^2}\right]^{-1}\mathbf{C}\mathbf{S}'\right]. \tag{6}$$

Here, we are interested in the two source case. For convenience, the signal coherence C_{12} is expressed as $C_{12} = c = |c|e^{j\phi}$. The array signal-to-noise ratios (ASNR) of the two sources are defined to be $A_1 = M(\sigma_1^2/\sigma_0^2)$ and $A_2 = M(\sigma_2^2/\sigma_0^2)$, respectively. The geometric mean of the ASNRs is $A_{12} = \sqrt{A_1 A_2}$. In this case, the correlation matrix and its inverse can be expressed, respectively, as

$$R = \sigma_0^2 \left[I + \frac{A_1}{M} \underline{S}_1 \underline{S}_1' + \frac{A_{12}}{M} \left[c \underline{S}_1 \underline{S}_2' + c^* \underline{S}_2 \underline{S}_1' \right] + \frac{A_2}{M} \underline{S}_2 \underline{S}_2' \right] \tag{7}$$

and

$$R^{-1} = \frac{1}{\sigma_0^2} \left[I - \frac{\tilde{A}_1}{M} \underline{S}_1 \underline{S}_1' - \frac{\tilde{A}_{12}}{M} \left[\tilde{c} \underline{S}_1 \underline{S}_2' + \tilde{c}^* \underline{S}_2 \underline{S}_1' \right] - \frac{\tilde{A}_2}{M} \underline{S}_2 \underline{S}_2' \right]. \tag{8}$$

The similarity in form of the correlation matrix and its inverse is readily apparent from equations (7) and (8). The parameters $\tilde{A}_1$, $\tilde{A}_2$ and $\tilde{c}$ are given by

$$\tilde{A}_1 = \frac{\left[1 + A_2(1-|c|^2) \right] A_1}{1+A_1+A_2+2A_{12}\mathrm{Re}\left[c^* \cos(\underline{S}_1, \underline{S}_2) \right] + A_1 A_2 (1-|c|^2) \left[1-\cos^2(\underline{S}_1, \underline{S}_2) \right]} \tag{9a}$$

$$\tilde{A}_2 = \frac{\left[1 + A_1(1-|c|^2) \right] A_2}{1+A_1+A_2+2A_{12}\mathrm{Re}\left[c^* \cos(\underline{S}_1, \underline{S}_2) \right] + A_1 A_2 (1-|c|^2) \left[1-\cos^2(\underline{S}_1, \underline{S}_2) \right]} \tag{9b}$$

$$\tilde{c} = \frac{c - A_{12}(1-|c|^2)\cos(\underline{S}_1, \underline{S}_2)}{\sqrt{(1 + A_1(1-|c|^2))(1 + A_2(1-|c|^2))}}. \tag{9c}$$

$\tilde{A}_1$ and $\tilde{A}_2$ are the modified ASNRs of the two sources. The geometric mean of the modified ASNRs is $\tilde{A}_{12} = \sqrt{\tilde{A}_1 \tilde{A}_2}$. As with coherence, the magnitude of the modified coherence, $\tilde{c}$, lies between zero and one. The modified coherence can be expressed in terms of its magnitude and phase: $\tilde{c} = |\tilde{c}| e^{j\tilde{\rho}}$. For equal-energy sources $A \equiv A_1 = A_2 = A_{12}$ and $\tilde{A} \equiv \tilde{A}_1 = \tilde{A}_2 = \tilde{A}_{12}$.

Finally, for the two source case, the matrix B_q^{-1} appearing in equation (3d) can be written as

$$B_q^{-1} = \frac{1}{\sigma_0^4}\begin{bmatrix} \underline{U}_q\underline{U}_q' - \frac{\tilde{A}_1}{M}\left[e^{j\alpha_{1,q}}\underline{U}_q\underline{S}_1' + e^{-j\alpha_{1,q}}\underline{S}_1\underline{U}_q'\right] - \frac{\tilde{A}_2}{M}\left[e^{j\alpha_{2,q}}\underline{U}_q\underline{S}_2' + e^{-j\alpha_{2,q}}\underline{S}_2\underline{U}_q'\right] \\ -\frac{\tilde{A}_{12}}{M}\left[\tilde{c}^* e^{j\alpha_{2,q}}\underline{U}_q\underline{S}_1' + \tilde{c}e^{-j\alpha_{2,q}}\underline{S}_1\underline{U}_q' + \tilde{c}e^{j\alpha_{1,q}}\underline{U}_q\underline{S}_2' + \tilde{c}^* e^{-j\alpha_{1,q}}\underline{S}_2\underline{U}_q'\right] \\ +\frac{\tilde{\tilde{A}}_1}{M^2}\underline{S}_1\underline{S}_1' + \frac{\tilde{\tilde{A}}_{12}}{M^2}\left[e^{j\tilde{\tilde{\phi}}}\underline{S}_1\underline{S}_2' + e^{-j\tilde{\tilde{\phi}}}\underline{S}_2\underline{S}_1'\right] + \frac{\tilde{\tilde{A}}_2}{M^2}\underline{S}_2\underline{S}_2' \end{bmatrix} \quad (10)$$

where the parameters $\tilde{\tilde{A}}_1$, $\tilde{\tilde{A}}_2$ and $\tilde{\tilde{\phi}}$ are given by

$$\tilde{\tilde{A}}_1 = \left|\tilde{A}_1 e^{-j\alpha_{1,q}} + \tilde{A}_{12}\tilde{c}e^{-j\alpha_{2,q}}\right|^2 \quad (11a)$$

$$\tilde{\tilde{A}}_2 = \left|\tilde{A}_2 e^{-j\alpha_{2,q}} + \tilde{A}_{12}\tilde{c}^* e^{-j\alpha_{1,q}}\right|^2 \quad (11b)$$

$$\tilde{\tilde{\phi}} = \text{angle}\left\{\left[\tilde{A}_1 e^{-j\alpha_{1,q}} + \tilde{A}_{12}\tilde{c}e^{-j\alpha_{2,q}}\right]\left[\tilde{A}_2 e^{j\alpha_{2,q}} + \tilde{A}_{12}\tilde{c}^* e^{j\alpha_{1,q}}\right]\right\}. \quad (11c)$$

$\tilde{\tilde{A}}_1$ and $\tilde{\tilde{A}}_2$ are the **doubly-modified ASNRs** of the two sources. The geometric mean of the doubly-modified ASNRs is $\tilde{\tilde{A}}_{12} = \sqrt{\tilde{\tilde{A}}_1\tilde{\tilde{A}}_2}$. For equal-energy sources $\tilde{\tilde{A}} \equiv \tilde{\tilde{A}}_1 = \tilde{\tilde{A}}_2 = \tilde{\tilde{A}}_{12}$.

3. Detection and Resolution of Source Bearing

To study the effect of source bearing, signal-to-noise ratio, and source coherence on the detection and resolution capabilities of the various array processing algorithms, we restrict our attention to the case where two equal-energy signals impinge on the array. For convenience, we define the complex cosine between two complex vectors to be

$$\cos(\underline{X},\underline{Y}) \equiv \frac{\underline{X}'\underline{Y}}{\|\underline{X}\|\|\underline{Y}\|}.$$

3.1. Resolution

When the sources are resolved, the beam energy evaluated at either target bearing must be larger than the beam energy evaluated between the target bearings. The between-targets direction-of-look vector, $\underline{W}_0$, is defined to have elements $W_{0m} = \exp\left[j(\alpha_{1,m}+\alpha_{2,m})/2\right]$. For a LES array, when the source bearings are symmetric about array broadside, the between-targets bearing-of-look lies halfway between the target bearings, i.e. at broadside. The criterion used for resolution of the sources is that the ratio of on-target to between-target beam energies exceed a threshold value of $\pi^2/8$. This quantity, known as the Rayleigh resolution limit, is the ratio obtained by the Bartlett algorithm using a LES array composed of many elements when the signal-to-noise ratio is large and the source bearing separation is equal to one beam-width. A beam-width is the bearing separation between the center of the main lobe and the first null of a classical beam-pattern.

The following formulae exactly express the dependence of the on-to-between-target beam energy ratios on ASNR, coherence, and bearing separation.

$$\frac{P_{BART}(on)}{P_{BART}(between)} = \frac{1 + A\left[1 + \cos^2(\underline{S}_1,\underline{S}_2) + 2|c|\cos(\phi)\cos(\underline{S}_1,\underline{S}_2)\right]}{1 + 2A\cos^2(\underline{W}_0,\underline{S}_1)\left[1 + |c|\cos(\phi)\right]} \tag{12}$$

$$\frac{P_{ME}(on)}{P_{ME}(between)} = \frac{1 - 2\tilde{A}\cos^2(\underline{W}_0,\underline{S}_1)\left[1 + |\tilde{c}|\cos(\tilde{\phi})\right]}{1 - \tilde{A}\left[1 + \cos^2(\underline{S}_1,\underline{S}_2) + 2|\tilde{c}|\cos(\tilde{\phi})\cos(\underline{S}_1,\underline{S}_2)\right]} \tag{13}$$

$$\frac{P_{LP_q}(on)}{P_{LP_q}(between)} = \left[\frac{\left[1 + 2\tilde{A}(1 + \cos(\tilde{\phi}))\cos^2(\underline{W}_0,\underline{S}_1) - 4\tilde{A}\left[|\tilde{c}|\cos\left[\frac{\alpha_{2,q}-\alpha_{1,q}}{2} - \tilde{\phi}\right] + \cos\left[\frac{\alpha_{2,q}-\alpha_{1,q}}{2}\right]\right]\right]}{\left[1 + \tilde{A}\left[1 + \cos^2(\underline{S}_1,\underline{S}_2) + 2\cos(\tilde{\phi})\cos(\underline{S}_1,\underline{S}_2)\right] - 2\tilde{A}\left[|\tilde{c}|(\cos(\alpha_{2,q}-\alpha_{1,q}-\tilde{\phi})+\cos(\tilde{\phi})) + 1 + \cos(\alpha_{2,q}-\alpha_{1,q})\cos(\underline{S}_1,\underline{S}_2)\right]\right]}\right]^{1/2} \tag{14}$$

These expressions are valid for all phase-centered arrays which exhibit symmetry through the origin. For such geometries, the complex cosines between the source and direction-

of-look vectors are real valued. The effects of array geometry, number of sensors, and source bearing separation are contained entirely in these cosine terms.

The complexity of expressions (12, 13, and 14) prevents a clear understanding of the effects of ASNR, coherence, and bearing separation on resolving capability. To gain such an understanding, numerical solutions were obtained for the resolvent array signal-to-noise ratio, the minimum ASNR which results in resolved sources. A LES array was assumed, and the sources were assumed to be located symmetrically about array broadside. The resolvent ASNR is a function of the magnitude and phase of the coherence as well as source bearing separation.

Figure 3a compares the minimum ASNR necessary for a ten element array to resolve the bearings of incoherent sources using the Bartlett, ME, and LP_0 processing algorithms. Of the three, the LP_0 algorithm requires the least ASNR to resolve source bearings. The ME and LP_0 algorithms are both capable of resolving arbitrarily closely-spaced source bearings if the ASNR is high enough. In contrast, the Bartlett algorithm is incapable of resolving bearings spaced more closely than one beam-width regardless of the ASNR. Figures 1a, b, and c illustrate Bartlett, ME, and LP_0 beam-patterns, respectively, which just resolve the indicated incoherent sources. In each case the ASNR is 10dB and the bearing separation is the smallest resolvable (from figure 3a). A sensible way to compare the capabilities of the algorithms to resolve coherent sources is to select the coherence phase which maximizes the resolvent ASNR for each source bearing separation. Thus the worst-case resolvent ASNR is sufficient to guarantee bearing resolution regardless of coherence phase; sources with particular coherence phases can usually be resolved at a somewhat lower ASNR. Figures 3b and c compare the worst-case resolvent ASNR for the three algorithms when the coherence magnitude is .7 and .99, respectively. As the magnitude of the coherence increases, the resolvent ASNR for the ME and LP_0 algorithms increases. The LP_0 algorithm retains its advantage over ME and Bartlett processing with regard to bearing resolution. The LP_0 algorithm consistently requires roughly 15dB less ASNR than the ME algorithm to resolve closely-spaced source bearings. The Bartlett algorithm again exhibits a minimum separation below which source bearings cannot necessarily be resolved; this limit increases as the magnitude of the coherence increases.

As discussed by Johnson [2], the linear predictive algorithm offers flexibility in the choice of prediction element q. Figure 4 compares the minimum ASNR necessary for a ten element array to resolve the bearings of incoherent sources using the linear predictive algorithm with prediction elements 0 to 4. As a function of prediction element q, the resolvent ASNR is symmetric about the center of the array. For closely-spaced source bearings ($\theta \leq 4^\circ$) the center prediction elements (q=4,5) require the least ASNR to resolve the source bearings. Figures 5a and b show the LP_4 and LP_0 beam-patterns, respectively, which result when incoherent sources separated by 2° impinge on a ten element array; the ASNR is 21 dB. As expected (figure 4), the LP_4 algorithm resolves the source bearings whereas the LP_0 algorithm does not. More widely-separated bearings ($4^\circ < \theta \leq 22^\circ$) are most easily resolved by prediction elements at the ends of the array (q=0,9). The sharp peaks in the plots for prediction elements 3-6 correspond to situations in which these LP algorithms produce spurious peaks in their beam-patterns at bearings between the actual target bearings. Figure 6 illustrates this phenomenon when q=3. While the source bearings are visibly resolved, peak bias and the spurious intermediate peak combine to confound the resolution criterion. For all prediction

elements, as source coherence increases in magnitude from zero to one, the resolvent ASNR rises quite uniformly as a function of bearing separation. For a ten element array, the resolvent ASNR for sources having .7 coherence magnitude is 6dB greater than for incoherent sources; the resolvent ASNR for sources having .99 coherence magnitude is 15dB greater.

3.2. Detection

In addition to resolving source bearings, it is necessary for a processing algorithm to detect the presence of sources by exhibiting peaks in the beam-pattern which stand out against off-target ripple. The criterion used for detection of the sources is that the ratio of on-target to highest-sidelobe beam energy exceed a threshold value of two. This ratio is established in two stages. First, the ratio of on-target beam energy to noise beam energy is established. By definition, the noise beam energy is evaluated when no sources are present, i.e. $A_1 = A_2 = 0$. Second, a relationship is established between the highest-sidelobe and noise beam energies. Together, these relationships are used to assess each algorithm's detection capability.

The following formulae exactly express the dependence of the on-target-to-noise beam energy ratios on ASNR, coherence, and bearing separation.

$$\frac{P_{BART}(on)}{P_{BART}(noise)} = 1 + A\left[1 + \cos^2(\underline{S}_1,\underline{S}_2) + 2|c|\cos(\phi)\cos(\underline{S}_1,\underline{S}_2)\right] \tag{15}$$

$$\frac{P_{ME}(on)}{P_{ME}(noise)} = \frac{1}{1 - \tilde{A}\left[1 + \cos^2(\underline{S}_1,\underline{S}_2) + 2|\tilde{c}|\cos(\tilde{\phi})\cos(\underline{S}_1,\underline{S}_2)\right]} \tag{16}$$

$$\frac{P_{LP_q}(on)}{P_{LP_q}(noise)} = \left[\frac{1}{\left[1 + \tilde{\tilde{A}}\left[1 + \cos^2(\underline{S}_1,\underline{S}_2) + 2\cos(\tilde{\tilde{\phi}})\cos(\underline{S}_1,\underline{S}_2)\right] - 2\tilde{\tilde{A}}\left[|\tilde{\tilde{c}}|(\cos(\alpha_{2,q}-\alpha_{1,q}-\tilde{\tilde{\phi}})+\cos(\tilde{\tilde{\phi}})) + 1 + \cos(\alpha_{2,q}-\alpha_{1,q})\cos(\underline{S}_1,\underline{S}_2)\right]\right]}\right]^{1/2} \tag{17}$$

These expressions are valid for all phase-centered arrays which exhibit symmetry through the origin. The effects of array geometry, number of sensors, and source bearing separation are contained entirely in the cosine terms.

For LES arrays it is straightforward to show that the worst-case (largest) ratios of highest-sidelobe-to-noise beam energy are:

$$\frac{P_{BART}(\text{highest sidelobe})}{P_{BART}(\text{noise})} = 1 + \frac{16A}{9\pi^2} \tag{18}$$

$$\frac{P_{ME}(\text{highest sidelobe})}{P_{ME}(\text{noise})} = \frac{1}{1 - \frac{16\tilde{A}}{9\pi^2}} \tag{19}$$

$$\frac{P_{LP_q}(\text{highest sidelobe})}{P_{LP_q}(\text{noise})} = \frac{1}{1 - \frac{8}{3\pi}\left[\tilde{A} + \frac{\tilde{\tilde{A}}}{3\pi}\right]} \tag{20}$$

Equations (15, 16, and 17) in conjunction with (18, 19, and 20) establish lower bounds on the on-target-to-highest-sidelobe beam energy ratios for LES arrays. Using these bounds, numerical solutions were obtained for the detectable array signal-to-noise ratio, the minimum ASNR which causes the ratio of on-target to highest-sidelobe beam energies to exceed the threshold value of two. As with the resolvent ASNR, the detectable ASNR is a function of the coherence magnitude and phase as well as source bearing separation. The detectable ASNR of the Bartlett algorithm is virtually unaffected by increasing source coherence. The LP algorithm requires the least ASNR to detect incoherent sources, while the Bartlett algorithm requires the highest. For coherent sources, the worst-case coherence phase maximizes the detectable ASNR. Thus the worst-case detectable ASNR is sufficient to guarantee source detection regardless of coherence phase; sources with particular coherence phases can usually be detected at a somewhat lower ASNR. As source coherence increases, the worst-case detectable ASNR for the ME and LP algorithms increases. For highly coherent sources, the LP algorithm requires the highest ASNR to guarantee source detection, and the Bartlett algorithm the least. All of the algorithms require a higher SNR to detect widely-separated sources than to resolve them. Conversely, all of the algorithms require a higher SNR to resolve closely-spaced sources than to detect them. Figures 7a, b, and c show the minimum ASNR required by the Bartlett, ME, and LP_0 processing algorithms to guarantee both detection and resolution of equal-energy sources with varying degrees of coherence.

4. Peak Bias

Even when targets can be detected and resolved in a background of white noise, the corresponding peaks in the beam-patterns may not occur at precisely the true source bearings (i.e., they may be biased). As passive sonar systems are often used to localize targets at great ranges, small errors in bearing estimates can lead to large errors in position estimates. In addition, non-zero bias would cause the resolvent and detectable ASNR of section 3 to be somewhat higher than necessary for visible peak resolution and/or detection. When a single source is present, all three algorithms yield an unbiased estimate of the source bearing when the correlation matrix is known; when multiple sources are present, the estimates are generally biased. In this section, formulae are presented which approximately describe the bias induced in one target peak by a second target for the Bartlett, ME, and LP beam-patterns. We emphasize that the bias results are based on

the assumption that the cross spectral correlation matrix is known exactly. Thus the formulae indicate the asymptotic (with respect to averaging) bias inherent in each processing algorithm.

We restrict our study of bias to LES arrays. The components of the direction-of-look vector are $W_m = \exp(-j(M-1-2m)\alpha/2)$, and the components of the source direction vectors are $S_{1m} = \exp(-j(M-1-2m)\alpha_1/2)$ and $S_{2m} = \exp(-j(M-1-2m)\alpha_2/2)$. The **transform bearing-of-look**, α, is related to the angular bearing-of-look, θ, by

$$\alpha = \pi \frac{d}{\lambda/2} \sin\theta,$$

where d is the sensor separation and λ is the signal wavelength. The source transform and angular bearings are similarly related.

The **transform bias** of the peak corresponding to source 1 is defined to be $\Delta\alpha_1 = \hat{\alpha}_1 - \alpha_1$, where $\hat{\alpha}_1$ is the estimate of the transform bearing of source 1, i.e. the location of the actual beam-pattern peak. The following notation will be used throughout the discussion:

$$g_1(\alpha) = M\cos\left[\underline{W},\underline{S}_1\right] = \frac{\sin(M(\alpha-\alpha_1)/2)}{\sin((\alpha-\alpha_1)/2)}$$

$$g_2(\alpha) = M\cos\left[\underline{W},\underline{S}_2\right] = \frac{\sin(M(\alpha-\alpha_2)/2)}{\sin((\alpha-\alpha_2)/2)}$$

Using equations (7) and (8), the Bartlett and ME beam-patterns can be expressed as functions of transform bearing as follows:

$$P_{BART}(\alpha) = \underline{W}'\underline{R}\underline{W} = \sigma_0^2\left[M + \frac{A_1}{M}g_1^2(\alpha) + 2\frac{A_{12}}{M}|c|\cos(\phi)g_1(\alpha)g_2(\alpha) + \frac{A_2}{M}g_2^2(\alpha)\right] \tag{21}$$

$$\left[P_{ME}(\alpha)\right]^{-1} = \underline{W}'\underline{R}^{-1}\underline{W} = \frac{1}{\sigma_0^2}\left[M - \frac{\tilde{A}_1}{M}g_1^2(\alpha) - 2\frac{\tilde{A}_{12}}{M}|\tilde{c}|\cos(\tilde{\phi})g_1(\alpha)g_2(\alpha) - \frac{\tilde{A}_2}{M}g_2^2(\alpha)\right] \tag{22}$$

When the bias is small compared to a beam-width, $2\pi/M$, Taylor series expansions of g_1, g_2, g_1^2, g_2^2, and g_1g_2 to second order about α_1 will be accurate in the neighborhood of the maximum. Substitution of these expansions into (21) and (22) and setting the derivatives with respect to α equal to zero at the maximum yields

$$\text{Bartlett:}\quad \Delta\alpha_1 = -\frac{\left[A_{12}|c|\cos(\phi)M + A_2 g_2(\alpha_1)\right] g_2'(\alpha_1)}{\left[\begin{array}{l} A_1 M g_1''(\alpha_1) + A_2\left[g_2'^2(\alpha_1) + g_2(\alpha_1)g_2''(\alpha_1)\right] \\ + A_{12}|c|\cos(\phi)\left[M g_2''(\alpha_1) + g_2(\alpha_1)g_1''(\alpha_1)\right] \end{array}\right]} \tag{23}$$

$$\text{ME:}\quad \Delta\alpha_1 = -\frac{\left[\tilde{A}_{12}|\tilde{c}|\cos(\tilde{\phi})M + \tilde{A}_2 g_2(\alpha_1)\right] g_2'(\alpha_1)}{\left[\begin{array}{l} \tilde{A}_1 M g_1''(\alpha_1) + \tilde{A}_2\left[g_2'^2(\alpha_1) + g_2(\alpha_1)g_2''(\alpha_1)\right] \\ + \tilde{A}_{12}|\tilde{c}|\cos(\tilde{\phi})\left[M g_2''(\alpha_1) + g_2(\alpha_1)g_1''(\alpha_1)\right] \end{array}\right]} \tag{24}$$

Taylor series analysis analogous to that already described is applied to the quadratic form (3d) to obtain the LP bias expression. For notational convenience, define $C_2(\alpha) = \cos(Q(\alpha-\alpha_2))$ and $S_2(\alpha) = \sin(Q(\alpha-\alpha_2))$, where $Q = (M-1-2q)/2$.

$$LP_q: \quad \Delta\alpha_1 = -\frac{\begin{bmatrix} \left[\tilde{\tilde{A}}_{12}\cos(\tilde{\tilde{\phi}})M+\tilde{\tilde{A}}_2 g_2(\alpha_1)\right]g_2'(\alpha_1) \\ - M\tilde{A}_2\left[C_2(\alpha_1)g_2'(\alpha_1)-QS_2(\alpha_1)g_2(\alpha_1)\right] \\ - M\tilde{A}_{12}|\tilde{c}|\cos(\tilde{\phi})\left[g_2'(\alpha_1)-MQS_2(\alpha_1)\right] \\ - M\tilde{A}_{12}|\tilde{c}|\sin(\tilde{\phi})\left[MQC_2(\alpha_1)-Qg_2(\alpha_1)\right] \end{bmatrix}}{\begin{bmatrix} \tilde{\tilde{A}}_1 Mg_1''(\alpha_1) + \tilde{\tilde{A}}_2\left[g_2(\alpha_1)g_2''(\alpha_1)+g_2'^2(\alpha_1)\right] \\ + \tilde{\tilde{A}}_{12}\cos(\tilde{\tilde{\phi}})\left[Mg_2''(\alpha_1)+g_1''(\alpha_1)g_2(\alpha_1)\right] \\ - M\tilde{A}_1\left[g_1''(\alpha_1)-MQ^2\right] \\ - M\tilde{A}_2\left[C_2(\alpha_1)g_2''(\alpha_1)-2QS_2(\alpha_1)g_2'(\alpha_1)-Q^2C_2(\alpha_1)g_2(\alpha_1)\right] \\ - M\tilde{A}_{12}|\tilde{c}|\cos(\tilde{\phi})\left[C_2(\alpha_1)g_1''(\alpha_1)-MQ^2C_2(\alpha_1)+g_2''(\alpha_1)-Q^2g_2(\alpha_1)\right] \\ - M\tilde{A}_{12}|\tilde{c}|\sin(\tilde{\phi})\left[S_2(\alpha_1)g_1''(\alpha_1)-MQ^2S_2(\alpha_1)-2Qg_2'(\alpha_1)\right] \end{bmatrix}} \tag{25}$$

Equations (23, 24, and 25) approximate the effects of source bearing separation, coherence, signal-to-noise ratio, relative source strength, and number of array elements on peak bias. While the expressions are complicated, several important observations can be made pertaining to each algorithm. For the Bartlett algorithm, bias does not depend on SNR. When the sources are incoherent, the bias of peak 1 increases as the strength of source 2 increases. The direction, positive or negative, of the bias depends on the source separation. While there are some bearing separations for which the bias is zero, generally it is non-zero. The behavior of ME peak bias as a function of relative source strength and coherence is clearly more complicated than is the Bartlett bias behavior (refer to eqs. (9) and (11)). However, the similarity of the ME and Bartlett bias expressions is obvious. For equal energy sources $\tilde{A}_1 = \tilde{A}_2$, and the only difference between equations (23) and (24) is the substitution of $\tilde{c}$ for c. The modified coherence ($\tilde{c}$) of sources which are not perfectly coherent tends asymptotically toward $-\cos(\underline{S}_1,\underline{S}_2) = -g_2(\alpha_1)/M$ as ASNR increases. Consequently the ME bias for equal-energy sources tends to zero as ASNR increases. However, for finite ASNR the ME bias is

generally non-zero. Similarly, it can be shown that the LP bias for equal-energy sources tends to zero as ASNR increases; for finite ASNR the LP bias is generally non-zero.

The complexity of the bias expressions necessitates computer evaluation. Figure 8a compares the Bartlett, ME, and LP_0 bias of two incoherent, equal-energy sources using a ten element array; the ASNR is 10dB. The approximately linear region of each plot for small source separations reflects the inability of the algorithms to resolve the sources. At larger source separations, the bias exhibits oscillatory behavior. The ME algorithm has the smallest amplitude of oscillation, followed by the LP_0 and Bartlett algorithms. In figure 8b, the ASNR has been raised to 30 dB. The bias of both the ME and LP_0 algorithms has decreased for all source separations; more closely-spaced sources are resolved than before. For widely-spaced sources, the ME bias remains smaller than the LP_0 bias. The Bartlett bias is unchanged by the increase in ASNR. Figures 9a, b, and c compare the Bartlett, ME, and LP_0 bias when the coherence magnitude is .7 and the ASNR is 10 dB. Each plot corresponds to a different coherence phase. Clearly coherence phase as well as source separation determine the direction and magnitude of the peak bias. For widely-separated sources, the Bartlett algorithm continues to exhibit the largest bias, and the ME algorithm the smallest.

Figure 10 compares the LP_q bias of incoherent source bearing produced by prediction elements 0-4 using a ten element array; the ASNR is 10dB. Note that the plot for the center prediction element (q=4) departs from linearity at a smaller source separation than the others, reflecting its superior resolution capability. However, the center prediction element can produce larger bias than the others for more widely-spaced sources.

When the sources are separated by at least an amount corresponding to the first zeros of (23, 24, and 25), the biases predicted by these expressions are very accurate. However expressions (23, 24, and 25) do not predict the biases of more closely-spaced sources accurately. The bias for unresolved sources can be a significant fraction of one beam-width. Consequently the validity of the bias expressions for closely-spaced sources is suspect because they are based on Taylor expansions of the beam-patterns to second order. Expansion of the beam-patterns to third order produces significantly more complicated bias expressions which do not provide a correspondingly great improvement in accuracy.

5. Effects of Finite Averaging

Results presented in sections 3 and 4 were based on use of the true correlation matrix. The effect of empirical computation of the correlation matrix by averaging the available sensor output data must also be considered. Assume that T=NK samples of the sensor outputs are available. The data is broken into K consecutive non-overlapping segments each of length N. The k^{th} data segment is transformed yielding a vector of Fourier transforms $\underline{X}^{(k)}(f)$. Following common practice [7,8], the correlation matrix estimate is given by:

$$\mathbf{R} = \frac{1}{K} \sum_{k=0}^{K-1} \underline{X}^{(k)}(f) \underline{X}^{(k)'}(f)$$

The statistics of this random matrix have been studied by Goodman[7]. It is important to note that R will not be positive definite or iinvertible if K < M because it will have M-K eigenvalues equal to zero.

Consider the following narrowband signal model:

$$s_p(nT) = \bar{\sigma}_p \, e^{j(2\pi f_p nT + \phi_p(nT))}$$

where f_p is the center frequency of source p and $\phi_p(t)$ is a slowly varying random phase. It is assumed that $\phi_p(t)$ varies slowly enough that it can be considered essentially constant over a length N DFT.

5.1. Coherence

Evaluating the DFT of the k^{th} signal segment at the analysis frequency f yields

$$\Psi_p^{(k)}(f) = \sigma_p \, e^{j\left[\phi_{p,k} + k2\pi f_p TN + \pi(f_p - f)T(N-1)\right]}$$

where $\phi_{p,k} = \phi_p(kNT)$ and σ_p is as defined in equation (2). The coherence coefficient between sources p and m is defined to be

$$C_{pm} \triangleq \frac{\frac{1}{K}\sum_{k=0}^{K-1} \Psi_p^{(k)} \Psi_m^{(k)*}}{\sigma_p \sigma_m}. \tag{26}$$

As $\Psi_p^{(k)}$ and $\Psi_m^{(k)}$ are random variables, so are the coherence coefficients. Comparing equations (26) and (4), it is apparent that the expectation operator has been replaced by a time average of the sample functions.

One important mechanism which results in source coherence is multipath propagation. To see how the coherence due to multipath depends on the time-bandwidth product, K, consider the two source case. The effect of multipath propagation is modelled by writing

$$\phi_{1,k} - \phi_{2,k} = \phi + \phi_k$$

where ϕ is a constant random phase shift due to the average difference in path lengths, and ϕ_k is a zero mean random phase variable which accounts for a time varying difference in path lengths due to platform motion, source motion, or motion of the scattering surface (see figure 11). For mathematical convenience, assume that ϕ_i and ϕ_k are statistically independent when $i \neq k$, and that the probability density of ϕ_k is uniform over the interval $[-\mu\pi, \mu\pi]$. The conditional expected value of the coherence given ϕ is

$$E(C_{12}|\phi) = \frac{\sin(\mu\pi)}{\mu\pi} \frac{\sin(\pi(f_1 - f_2)TNK)}{K\sin(\pi(f_1 - f_2)TN)} \, e^{j\left[\phi + \pi(f_1 - f_2)T(NK-1)\right]} \tag{27}$$

The magnitude of the conditional expected value of C_{12} is always less than or equal to one. It tends toward zero, but not monotonically, as the time-bandwidth product and/or the inter-signal frequency difference and/or the randomness of the inter-signal phase increases ($\mu \rightarrow 1$). The coherence between sources which have nearly the same center frequencies or phases is reduced by increasing the amount of averaging K. If the signals share the same center frequencies and have a constant phase relationship then the coherence magnitude will be one regardless of the amount of averaging performed. Even when the inter-signal phase sequence is completely random ($\mu = 1$) the variance of the magnitude of the coherence is 1/K, not zero. Thus sources which are incoherent in the expected value sense of equation (4) may not be incoherent in the time average sense of equation (26).

5.2. Randomness of Beam-Patterns

Capon and Goodman[8] have studied the statistics of the Bartlett and ME beam-patterns when finite averaging is performed to obtain the correlation matrix estimate, and Baggeroer[9] has studied the statistics of the LP spectral estimator for time series data. These analyses are rigorous mathematically, but fail to provide a simple guide to the amount of averaging required to reduce beam-pattern randomness to acceptable levels. By analyzing the variability of on-target and noise beam energies with respect to the non-zero signal-noise cross terms in the single source case [10], the following guidelines can be established which dictate the amount of averaging necessary for each algorithm to produce beam-patterns with a small random component. These results are valid for LES arrays.

$$\text{Bartlett:} \quad K \gg \frac{M}{\left[\frac{\sigma_0}{\sigma_1} + M\frac{\sigma_1}{\sigma_0}\right]^2} \tag{28}$$

$$\text{ME:} \quad K \gg M \tag{29}$$

$$\text{LP:} \quad K \gg M \text{ and } K \gg M^2\frac{\sigma_1^2}{\sigma_0^2} \tag{30}$$

Figures 12a, b, and c show several Bartlett beam-patterns for a ten element array when K=10, 100, and 1000, respectively; the SNR is one. The variability of the Bartlett beam-patterns decreases as K increases. In all three cases the amount of averaging is such that the criterion K>>.1 is satisfied. For K=10 the degree of variability is greater than might be expected; with such small time-bandwidth products the assumptions leading to condition (28) are not entirely valid; nevertheless the variability for K=10 is not so severe as to obscure the target. The variability of both the K=100 and K=1000 beam-patterns is small. Figures 13a, b, and c show the ME beam-patterns for the same data. The variability of the ME beam-patterns decreases as K increases. The K=10 case does not satisfy condition (29), and the variability is so great as to obscure the broadside target.

Figures 14a, b, and c show several LP_0 beam-patterns for a ten element array when K=10, 100, and 1000, respectively; the SNR is one. The variability of the patterns decreases as the time-bandwidth product increases. It has been shown [10] that finite averaging can also produce spurious noise induced peaks off-target in LP beam-patterns;

such peaks are apparent for the K=10 case. Only the K=1000 beam-pattern has small variability, as expected, since M^2=100. The second condition of (30) indicates that as the SNR increases, more averaging must be performed to maintain a constant level of noise induced variability in the beam energies. Figure 15 shows several LP_0 beam-patterns for a ten element array when K=1000; the array SNR is 20dB. Comparison of figures 14c and 15 confirms that the variability of the on-target beam energy increases as the SNR increases. For large arrays, the second condition (30) is dominant because of its proportionality to M^2.

6. Conclusions

The bearing estimation capabilities of the beamforming and linear predictive array processing algorithms discussed here are adversely affected by source coherence and by limited averaging in the computation of the correlation matrix. Furthermore, the performance of each algorithm is affected to a different degree by these conditions. For LES arrays, **no one algorithm is superior to the others in all situations.** Consequently, the coherence and amount of averaging possible in particular applications greatly influence the choice of an "optimal" array processing algorithm.

The incremental effect of a change in coherence magnitude on the detection and resolution capabilities and bias of the ME and LP algorithms is greatest when the coherence magnitude is large (near one); for the Bartlett algorithm, the incremental effect is greatest when the coherence magnitude is small. Thus, the adaptive algorithms (ME and LP) are less sensitive to low levels of signal coherence than is conventional beamforming. As the magnitude of the coherence increases from zero to one, the resolving capability of all of the algorithms diminishes. Except for perfectly coherent sources, the LP processing algorithm is uniformly the most capable of resolving closely-spaced sources, followed by ME and Bartlett processing. The superior resolution capability of the LP algorithm, compared with the ME algorithm, is somewhat offset by the greater bias of its bearing estimates. In terms of statistical averaging, **the Bartlett, ME, and LP algorithms do not yield asymptotically unbiased estimates of source bearing.** Therefore, Cramer-Rao lower bounds on the variance of these bearing estimates are suspect as they usually assume that the estimates are asymptotically unbiased. The version of this bound that pertains to biased estimators contains an additional factor of one plus the derivative of the bias with respect to the parameter being estimated [11]. Even for small biases, the magnitude of this derivative can be large with respect to one because of the oscillatory nature of the bias. For LES arrays the maximum magnitude of this slope appears to be independent of the number of array elements when the ASNR remains constant. The ME algorithm produces the least bias in its bearing estimates, and that bias decreases as SNR increases. LP bias is greater than ME bias, but also diminishes with increasing SNR. Bartlett bias is the most severe and is independent of SNR. The bias produced by all three algorithms becomes more severe as source coherence increases. The LP algorithm has a slightly greater capability to detect incoherent sources than the ME and Bartlett algorithms. Coherence has negligible effect on the detection capability of Bartlett processing. In contrast, as source coherence increases, the detection capability of ME processing decreases, as Seligson [5] observed. As source coherence increases, the LP algorithm becomes the least capable of detecting sources, and the Bartlett algorithm most capable. Thus a tradeoff exists between the resolution and detection of highly coherent sources.

The variation to the LP algorithm of utilizing different prediction elements proves to be of some value. Moving the prediction element from the end to the center of a LES array enhances the capability of the linear predictive algorithm to resolve extremely closely-spaced source bearings. However, the beam-patterns produced by the center

prediction elements are more likely to exhibit spurious peaks when the sources are less closely spaced. In addition, bias of the bearing estimates can be greatest when the center prediction elements are utilized. Choice of prediction element has no effect on the capability of the LP algorithm to detect widely-separated sources. The effect of increasing source coherence is the same for all prediction elements.

In section 5 constraints on the time-bandwidth product were presented which ensure minimal sensitivity of the beam-patterns to imperfections in the correlation matrix that result from finite averaging. The Bartlett beam-pattern is least sensitive to finite averaging while LP beam-patterns are most sensitive. The sensitivity of the ME beam-pattern to finite averaging lies between these extremes. Thus, a tradeoff exists between resolving capability and sensitivity to finite averaging.

The LP algorithms are most capable of resolving closely-spaced sources; however, their high sensitivity to finite averaging restricts their application to environments where large amounts of averaging are possible. The Bartlett algorithm is least sensitive to finite averaging and requires the least SNR to detect widely-separated sources; however, its resolving capability is very poor. The ME algorithm lies between the LP and Bartlett algorithms in terms of resolution and detection capabilities as well as sensitivity to finite averaging. In addition, the ME algorithm produces the least biased estimates of source bearing. Thus the ME algorithm seems best suited to applications where the amount of averaging possible is small and the capability to resolve closely-spaced source bearings is requisite. The LP algorithms are of little value in these situations because of their extreme sensitivity to noise. The Bartlett algorithm is also of little value here because of its extremely poor resolving capability. Table 1 crudely suggests which array processing algorithm is best suited to each of four combinations of source separation and amount of averaging possible when a LES array is used.

Time-bandwidth product	Bearing separation of sources	
	Closely spaced	Widely separated
Small	ME for all coherences	Bartlett for all coherences
Large	LP_{end} for all coherences LP_{center} for all coherences when signals are very close	Bartlett for all coherences LP or ME for small coherences

Table 1.
Suggested processing algorithms for LES arrays.

Figure Captions

Figure 1: Bartlett (a), ME (b), and LP_0 (c) beam-patterns generated using a ten element LES array with half-wavelength sensor spacing. The ASNR is 10dB, and the indicated sources are just resolved.

Figure 2: Array geometry which is symmetric through the origin.

Figure 3: Worst-case resolvent ASNR for the ten element LES array when the coherence magnitude is 0 (a), .7 (b), and .99 (c).

Figure 4: Dependence of linear predictive resolvent ASNR on prediction element using the ten element LES array. The sources are incoherent.

Figure 5: LP_4 (a) and LP_0 (b) beam-patterns that result when incoherent plane waves separated by 2° impinge on the ten element LES array. The ASNR is 21 dB.

Figure 6: LP_3 beam-pattern that results when incoherent plane waves separated by 14.023° impinge on the ten element LES array. The ASNR is 30 dB. The peak at 0° is spurious.

Figure 7: Worst-case resolvent and detectable ASNR for the ten element LES array when the coherence magnitude is 0 (a), .7 (b), and .99 (c).

Figure 8: Bias of incoherent source bearing estimates using the ten element LES array when the ASNR is 10dB (a) and 30dB (b)

Figure 9: Bartlett (a), ME (b), and LP_0 (c) bearing estimate biases for sources with coherence magnitude .7 using the ten element LES array. Each plot corresponds to a different coherence phase. The ASNR is 10 dB.

Figure 10: Dependence of linear predictive bearing estimate bias on prediction element using the ten element LES array. The sources are incoherent, and the ASNR is 10 dB.

Figure 11: Multipath propagation in the ocean due to specular reflection. The difference in path lengths varies as a function of time because of the dynamic ocean surface.

Figure 12: Variability of Bartlett beam-patterns induced by finite averaging. Each plot shows four beam-patterns corresponding to distinct estimates of the correlation matrix using the ten element LES array. The time-bandwidth product is 10 (a), 100 (b), and 1000 (c). The ASNR is 10 dB.

Figure 13: Variability of ME beam-patterns induced by finite averaging. Each plot shows four beam-patterns corresponding to distinct estimates of the correlation matrix using the ten element LES array. The time-bandwidth product is 10 (a), 100 (b), and 1000 (c). The ASNR is 10 dB.

Figure 14: Variability of LP_0 beam-patterns induced by finite averaging. Each plot shows four beam-patterns corresponding to distinct estimates of the correlation matrix using the ten element LES array. The time-bandwidth product is 10 (a), 100 (b), and 1000 (c). The ASNR is 10 dB.

Figure 15: Variability of LP_0 beam-patterns when the time-bandwidth product is 1000 and the ASNR is 20 dB. The variability of the on-target beam energy increases as the SNR increases.

References

[1] J. Capon, "High-Resolution Frequency-Wavenumber Spectrum Analysis", Proc. IEEE, vol. 57, pp. 1408-1418, Aug. 1969.

[2] D. H. Johnson, "The Application of Spectral Estimation Methods to Bearing Estimation Problems", Proc. IEEE, vol. 70, no. 10, Sept. 1982.

[3] H. Cox, "Resolving power and sensitivity to mismatch of optimum array processors", J. Acoust. Soc. Am. vol. 54(3), pp. 771-785, March 1973.

[4] C. D. Seligson, "Comments on 'High-Resolution Frequency-Wavenumber Analysis '", Proc. IEEE, vol. 58, pp. 947-949, June 1970.

[5] R. J. Urick, Principles of Underwater Sound, pp. 93-180, McGraw-Hill, New York, NY, 1975.

[6] A. S. Householder, The Theory of Matrices in Numerical Analysis, pp. 123-124, Dover Publications, Inc., New York, NY, 1964.

[7] N. R. Goodman, "Statistical Analysis Based on a Certain Multivariate Complex Gaussian Distribution", Ann. Math. Stat., vol. 34, pp. 152-177, March 1963.

[8] J. Capon, N. R. Goodman, "Probability Distributions for Estimators of the Frequency-Wavenumber Spectrum", Proc. IEEE, vol. 58, pp. 1785-1786, Oct. 1970.

[9] A. B. Baggeroer, "Confidence Intervals for Regression (MEM) Spectral Estimates", IEEE Trans. Inform. Theory, vol. IT-22, pp. 534-545, Sept. 1976.

[10] S. R. De Graaf, "The Effect of Coherent Signals on the Capability of Array Processing Algorithms to Resolve Source Bearings", M. S. Thesis, Dept. of Elec. Eng., Rice University, Houston, TX, 1982.

[11] H. Cramer, Mathematical Methods of Statistics, Princeton University Press, Princeton, NJ, 1946.

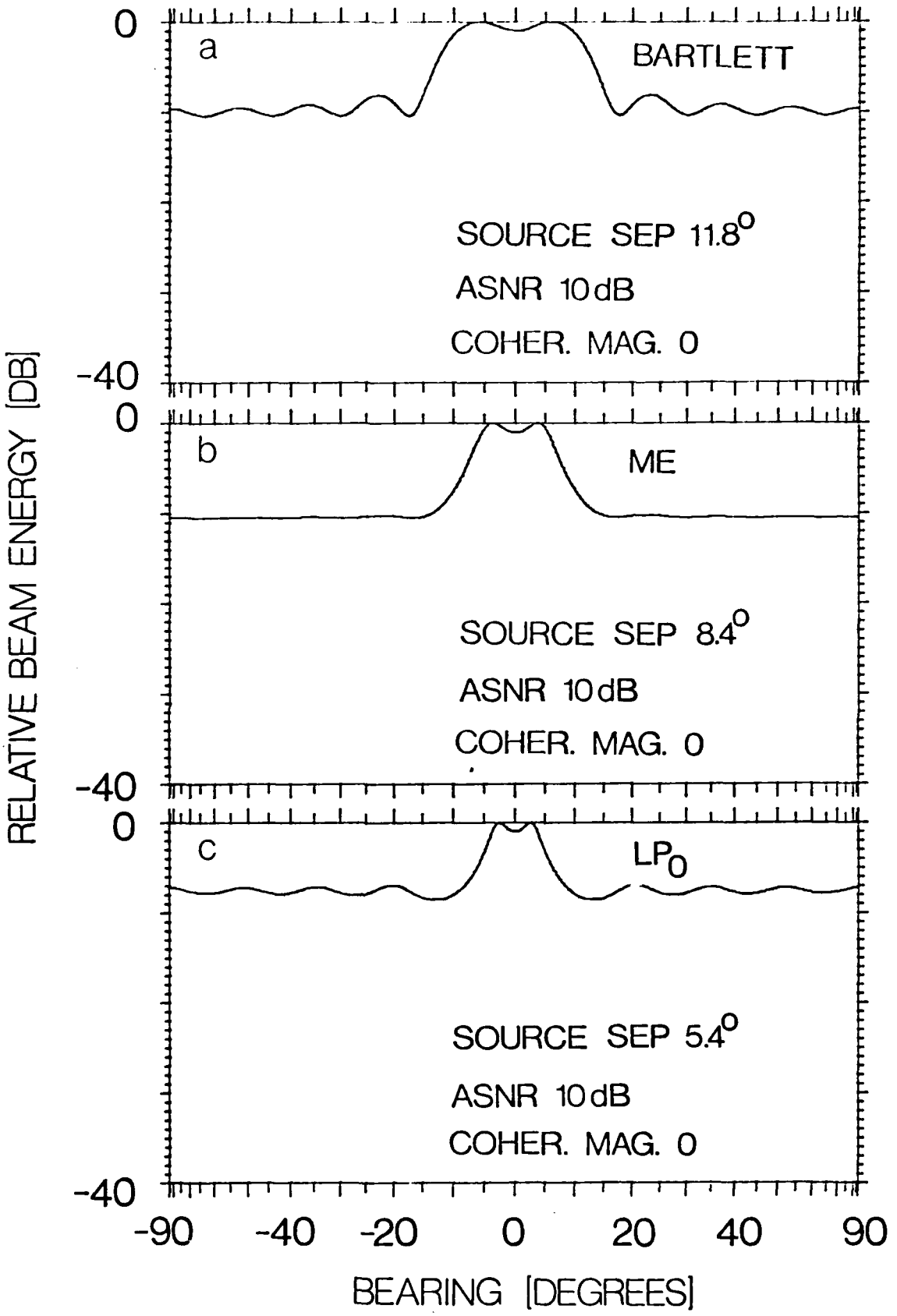
0
a
BARTLETT
SOURCE SEP 11.8°
ASNR 10dB
COHER. MAG. 0
-40
0
b
ME
SOURCE SEP 8.4°
ASNR 10dB
COHER. MAG. 0
-40
0
c
LP0
SOURCE SEP 5.4°
ASNR 10dB
COHER. MAG. 0
-40
RELATIVE BEAM ENERGY [DB]
-90
-40
-20
0
20
40
90
BEARING [DEGREES]

FIGURE 1

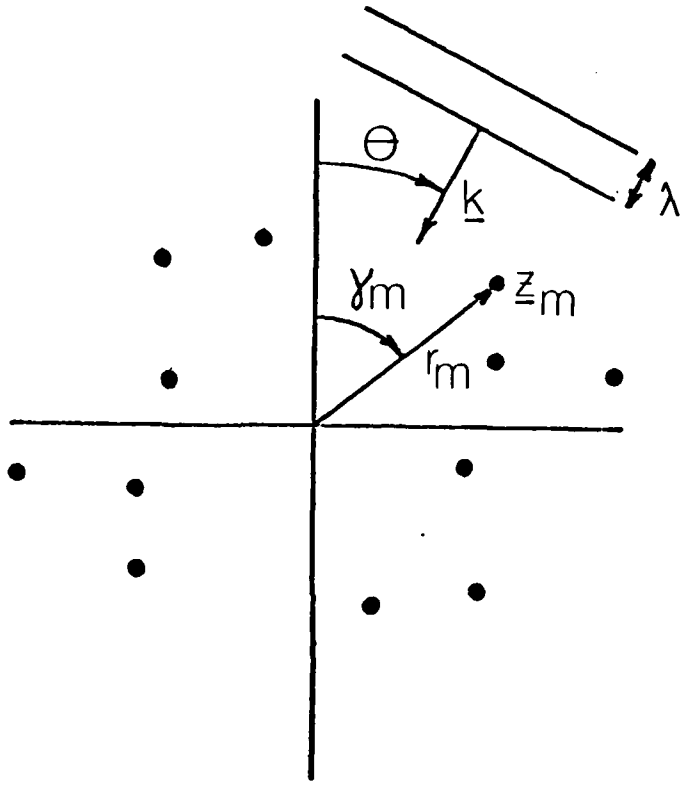

FIGURE 2

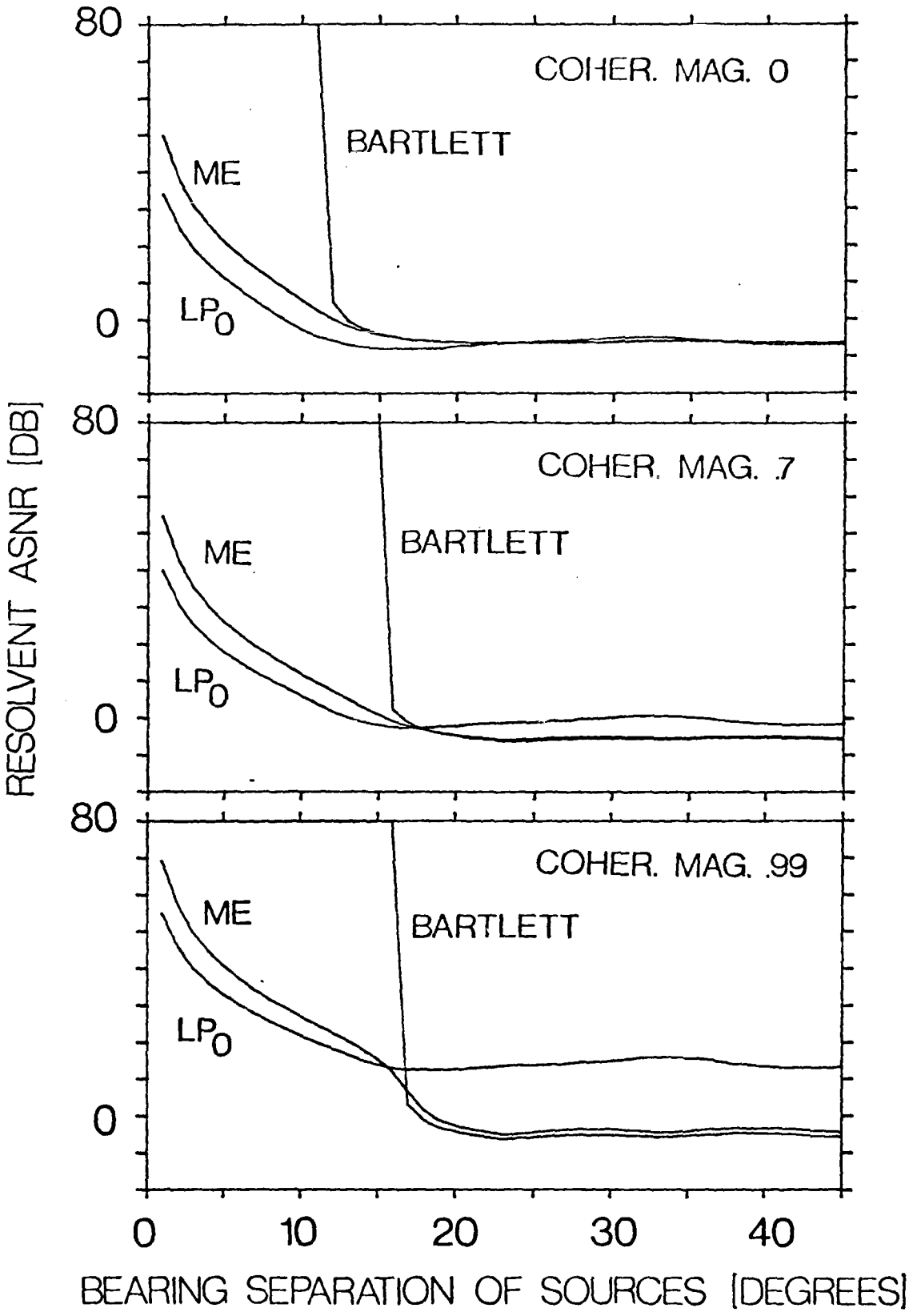
80
COHER. MAG. 0
BARTLETT
ME
LP0
0
80
COHER. MAG. .7
ME
BARTLETT
LP0
0
80
COHER. MAG. .99
ME
BARTLETT
LP0
0
RESOLVENT ASNR [DB]
0
10
20
30
40
BEARING SEPARATION OF SOURCES [DEGREES]

FIGURE 3

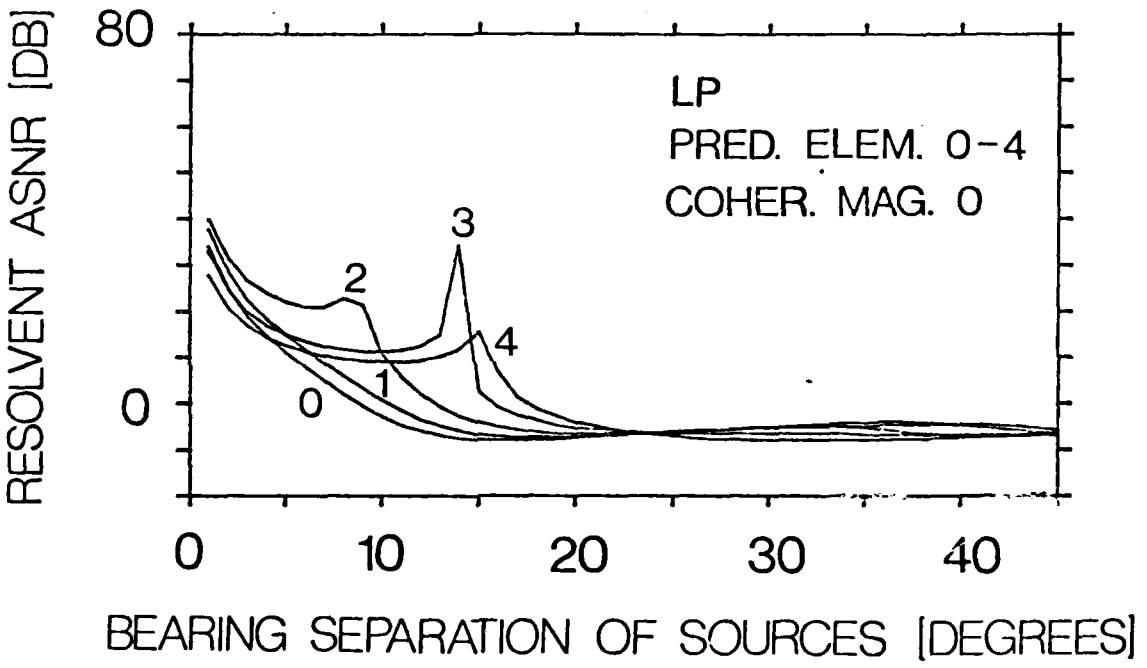
RESOLVENT ASNR [DB]
80
0
LP
PRED. ELEM. 0-4
COHER. MAG. 0
0
1
2
3
4
0
10
20
30
40
BEARING SEPARATION OF SOURCES [DEGREES]

FIGURE 4

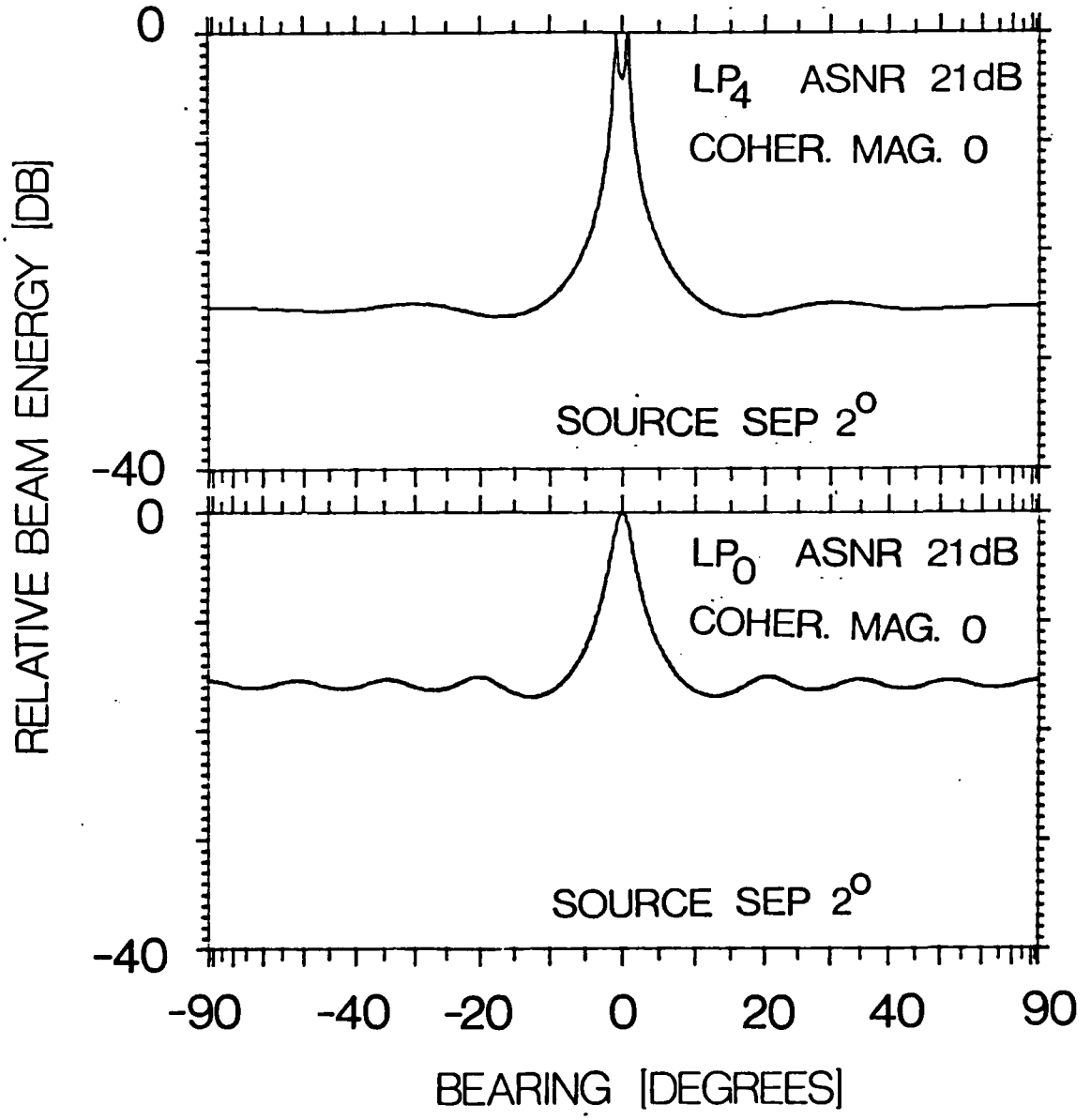
0
LP4 ASNR 21dB
COHER. MAG. 0
SOURCE SEP 2°
-40
0
LP0 ASNR 21dB
COHER. MAG. 0
SOURCE SEP 2°
-40
RELATIVE BEAM ENERGY [DB]
-90
-40
-20
0
20
40
90
BEARING [DEGREES]

FIGURE 5

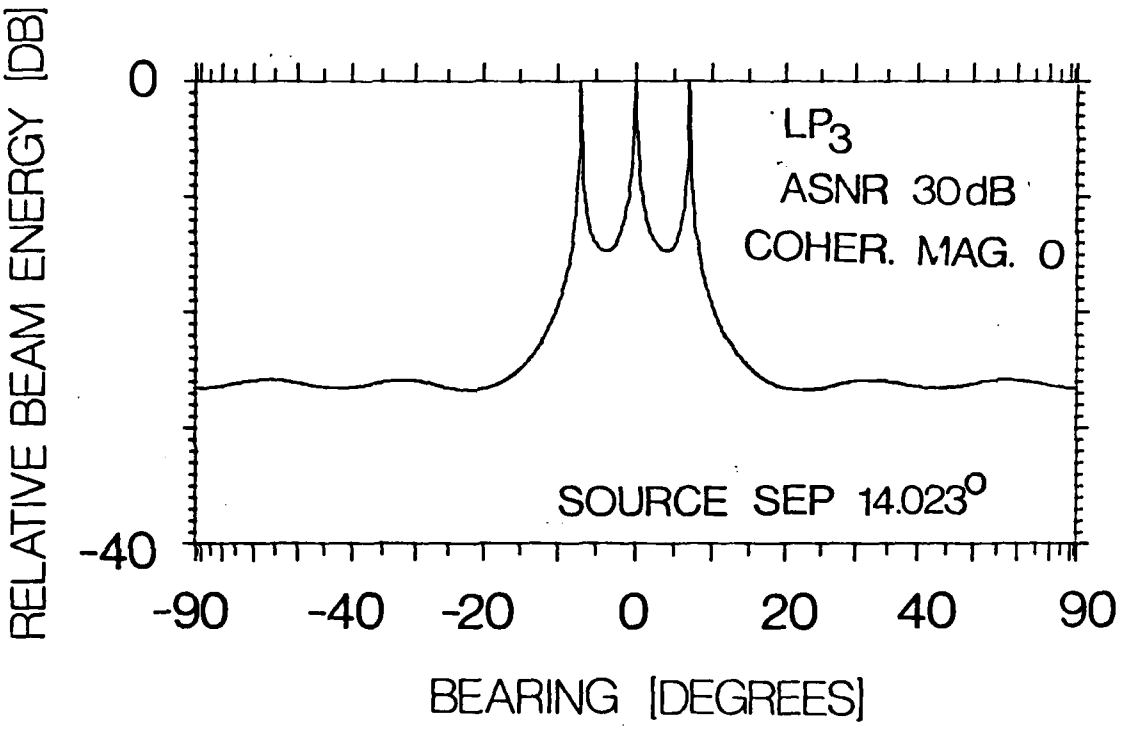
RELATIVE BEAM ENERGY [DB]
0
-40
LP3
ASNR 30dB
COHER. MAG. 0
SOURCE SEP 14.023°
-90
-40
-20
0
20
40
90
BEARING [DEGREES]

FIGURE 6

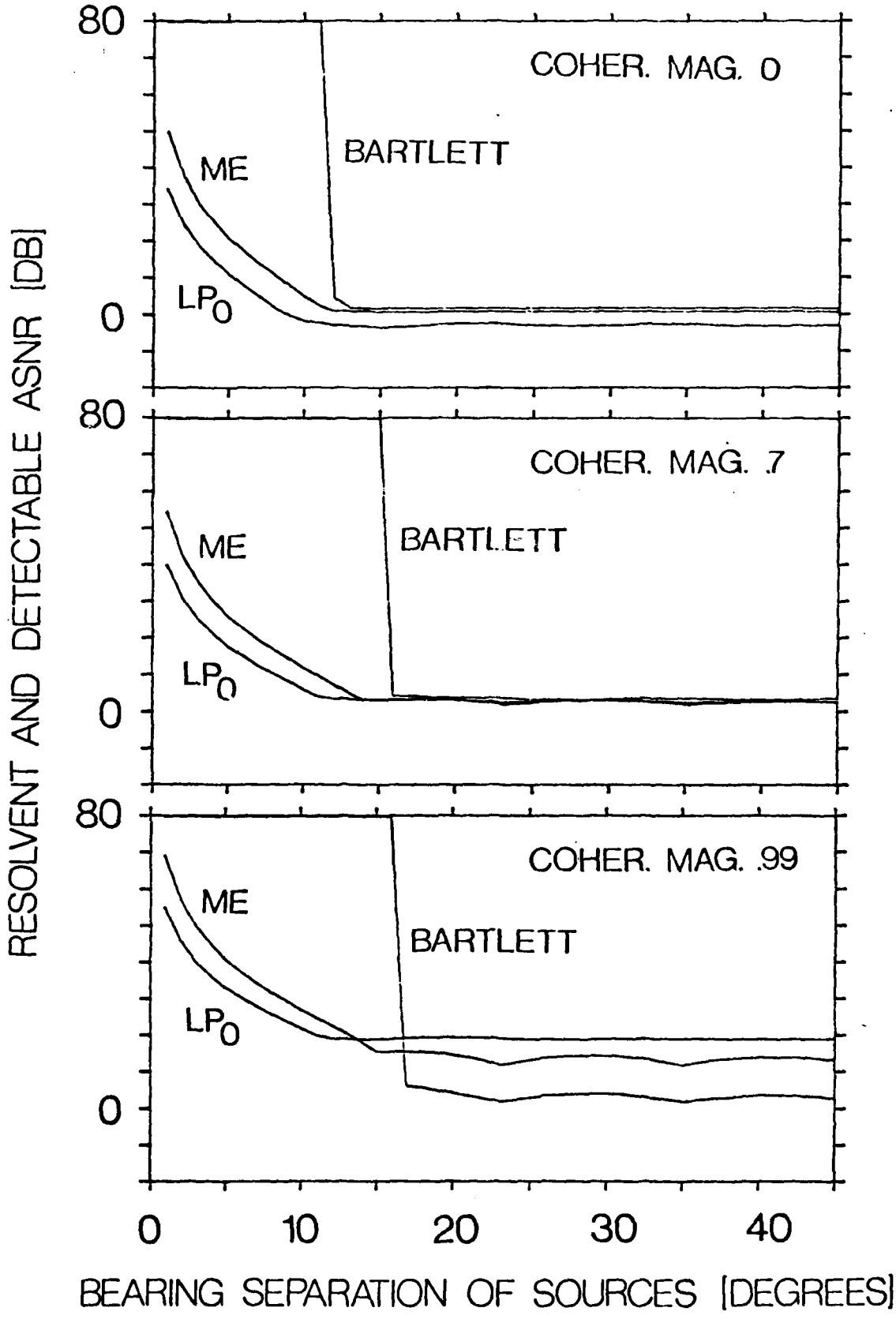
80
COHER. MAG. 0
BARTLETT
ME
LP0
0
80
COHER. MAG. .7
ME
BARTLETT
LP0
0
80
COHER. MAG. .99
ME
BARTLETT
LP0
0
0
10
20
30
40
RESOLVENT AND DETECTABLE ASNR [DB]
BEARING SEPARATION OF SOURCES [DEGREES]

FIGURE 7

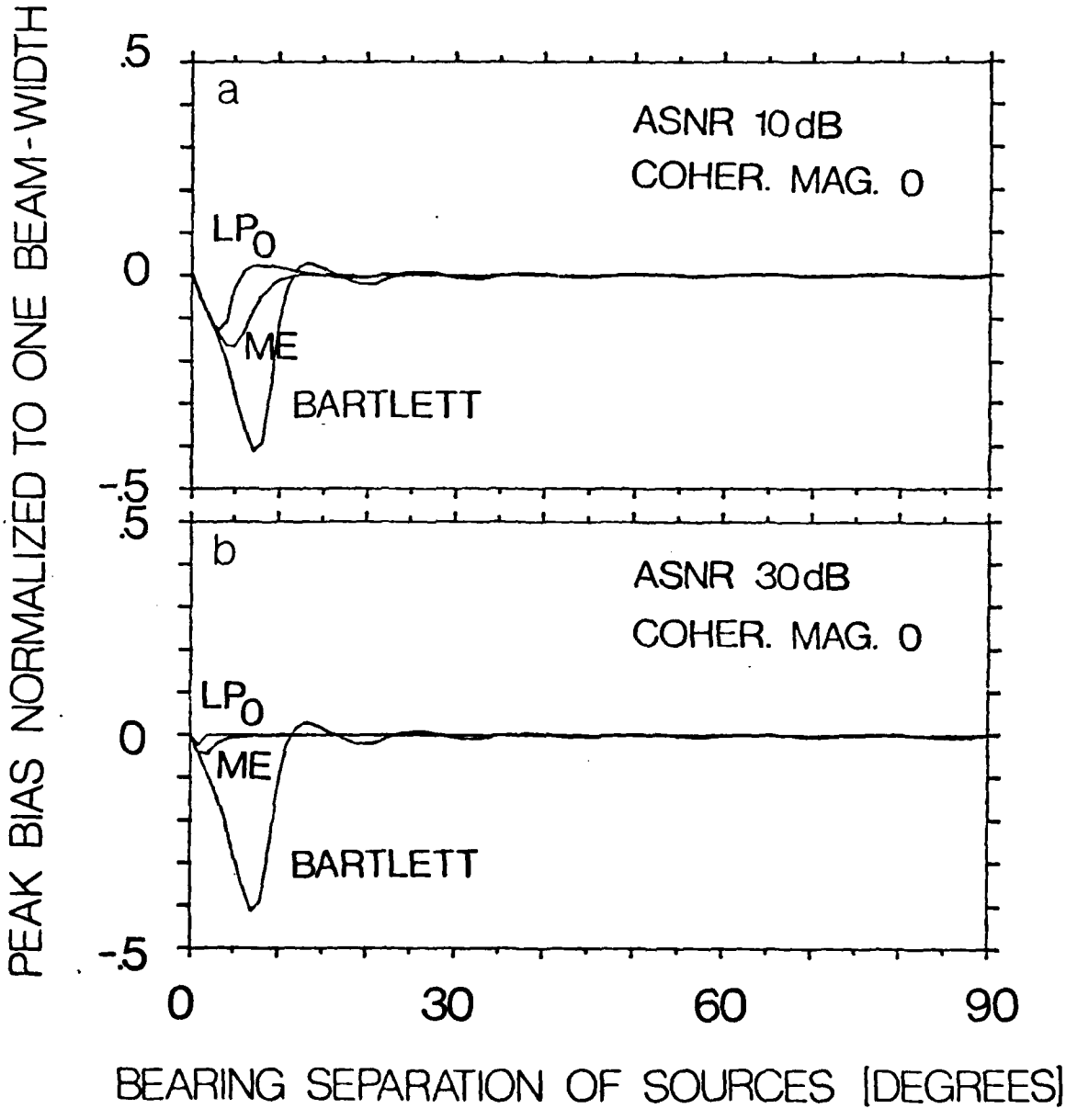
PEAK BIAS NORMALIZED TO ONE BEAM-WIDTH
.5
0
-.5
a
ASNR 10dB
COHER. MAG. 0
LP0
ME
BARTLETT
b
ASNR 30dB
COHER. MAG. 0
LP0
ME
BARTLETT
0
30
60
90
BEARING SEPARATION OF SOURCES [DEGREES]

FIGURE 8

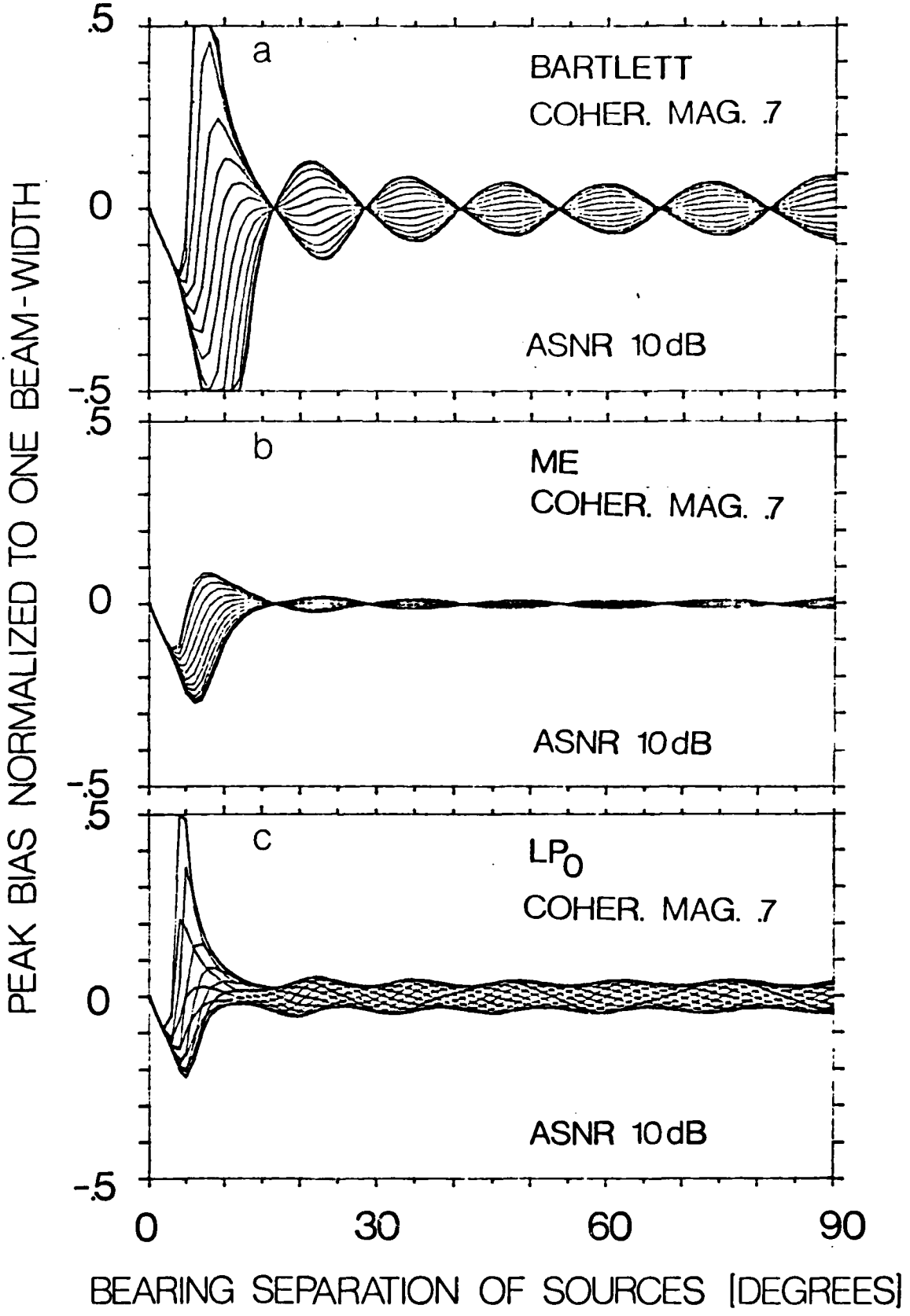
.5
0
-.5
a
BARTLETT
COHER. MAG. .7
ASNR 10dB
b
ME
COHER. MAG. .7
ASNR 10dB
c
LP0
COHER. MAG. .7
ASNR 10dB
PEAK BIAS NORMALIZED TO ONE BEAM-WIDTH
0
30
60
90
BEARING SEPARATION OF SOURCES [DEGREES]

FIGURE 9

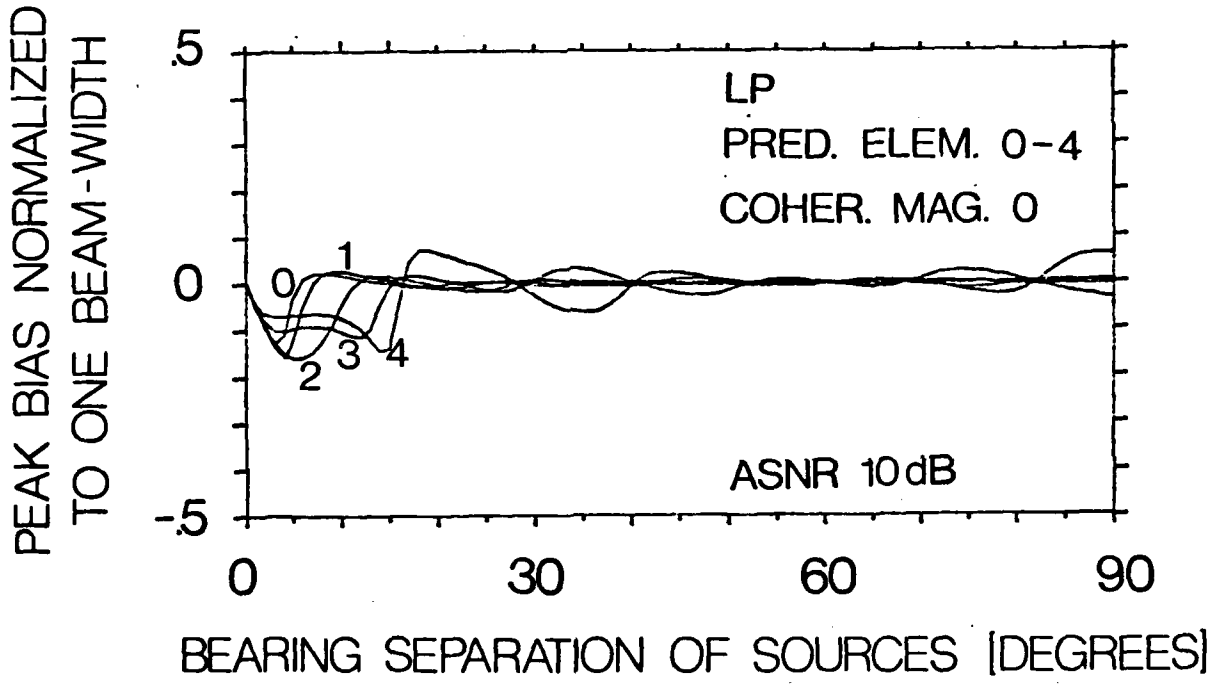
PEAK BIAS NORMALIZED
TO ONE BEAM-WIDTH
.5
0
-.5
0
30
60
90
LP
PRED. ELEM. 0-4
COHER. MAG. 0
ASNR 10dB
0
1
2
3
4
BEARING SEPARATION OF SOURCES [DEGREES]

FIGURE 10

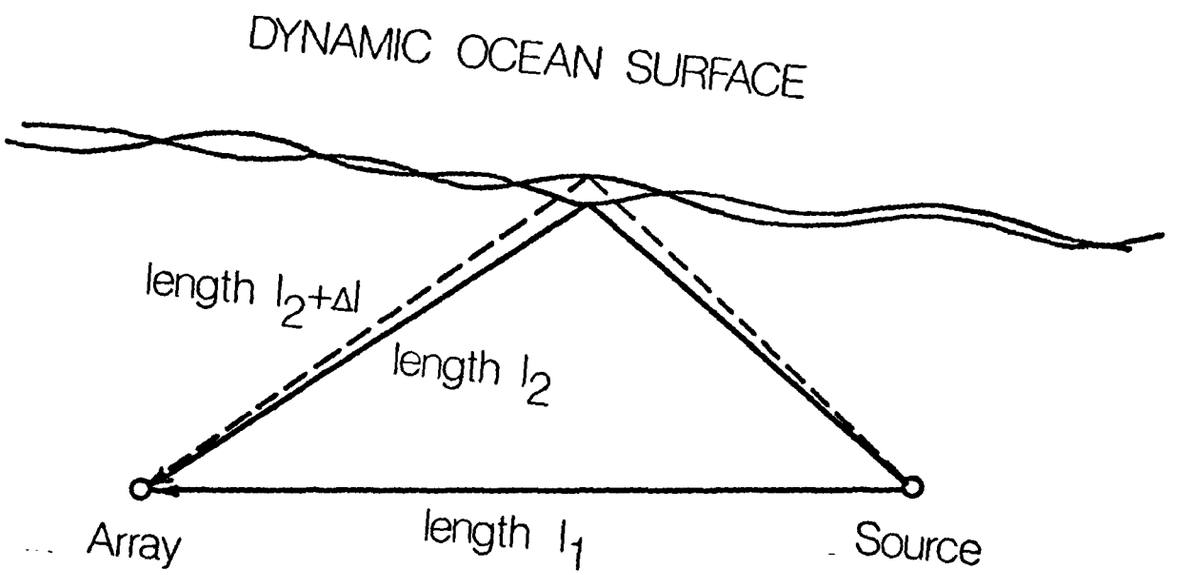
DYNAMIC OCEAN SURFACE
length $l_2+\Delta l$
length l_2
Array
length l_1
Source

FIGURE 11

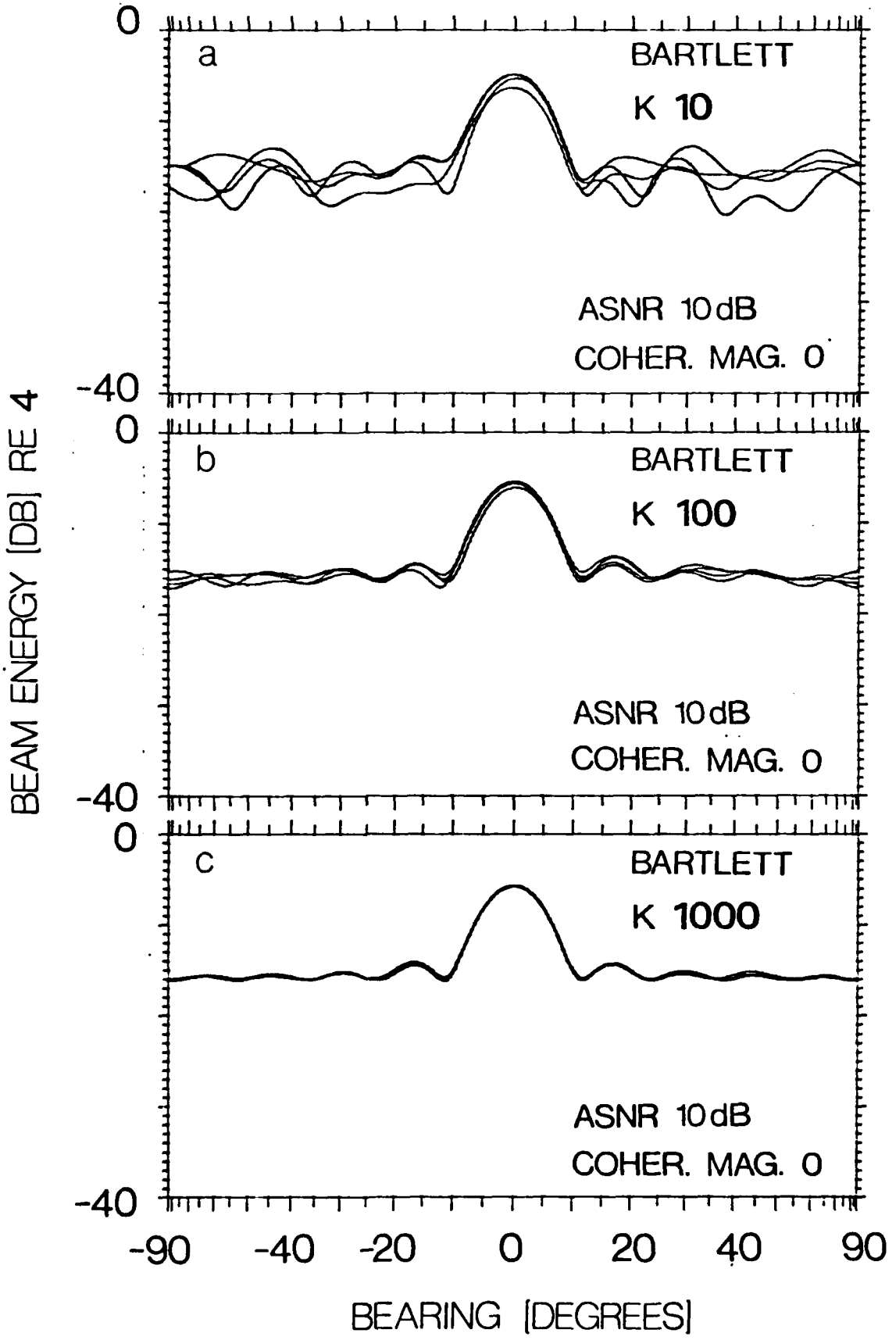
0
a
BARTLETT
K 10
ASNR 10dB
COHER. MAG. 0
-40
0
b
BARTLETT
K 100
ASNR 10dB
COHER. MAG. 0
-40
0
c
BARTLETT
K 1000
ASNR 10dB
COHER. MAG. 0
-40
BEAM ENERGY [DB] RE 4
-90
-40
-20
0
20
40
90
BEARING [DEGREES]

FIGURE 12

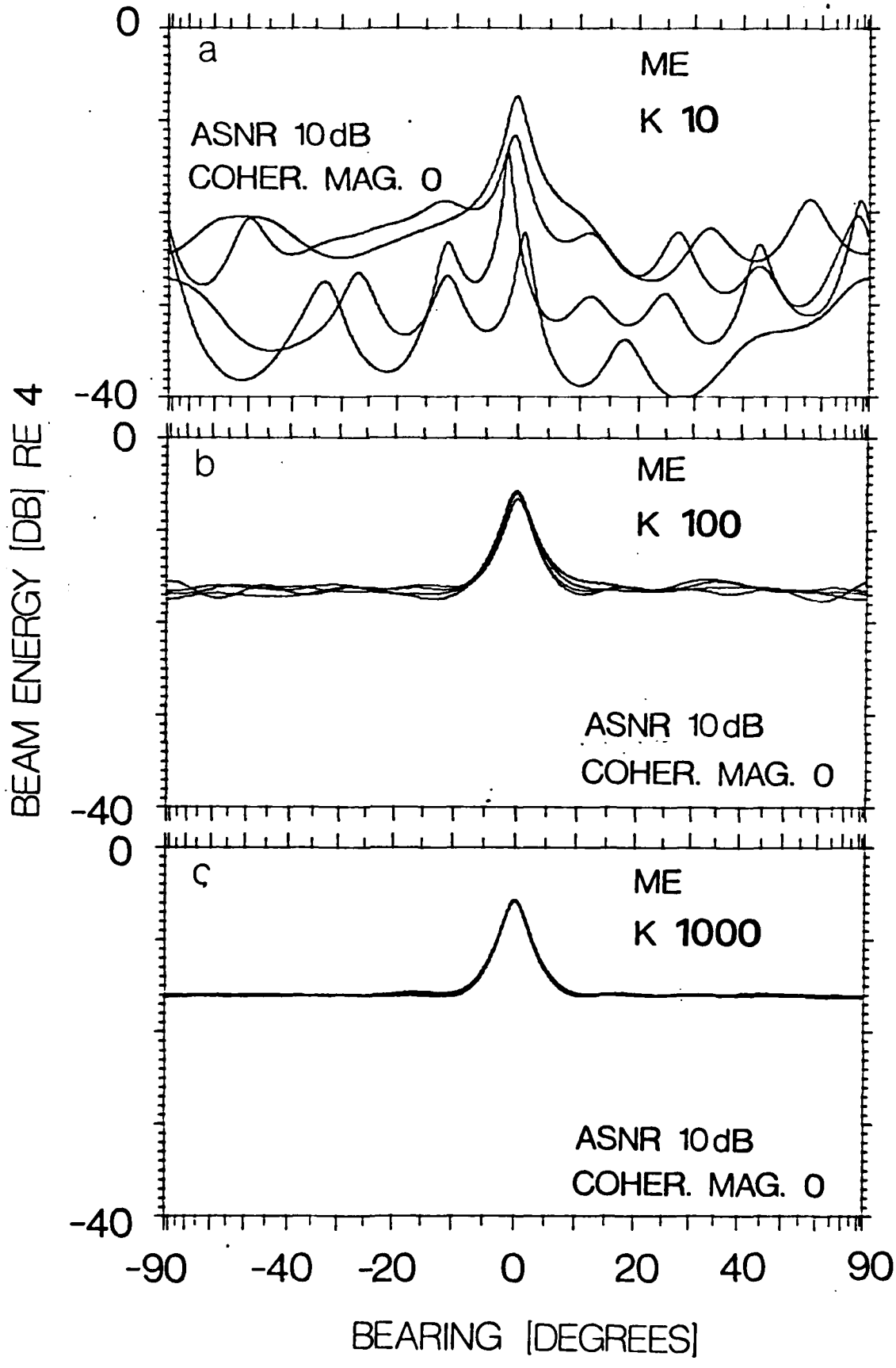
0
a
ME
K 10
ASNR 10dB
COHER. MAG. 0
-40
0
b
ME
K 100
ASNR 10dB
COHER. MAG. 0
-40
0
c
ME
K 1000
ASNR 10dB
COHER. MAG. 0
-40
BEAM ENERGY [DB] RE 4
-90
-40
-20
0
20
40
90
BEARING [DEGREES]

FIGURE 13

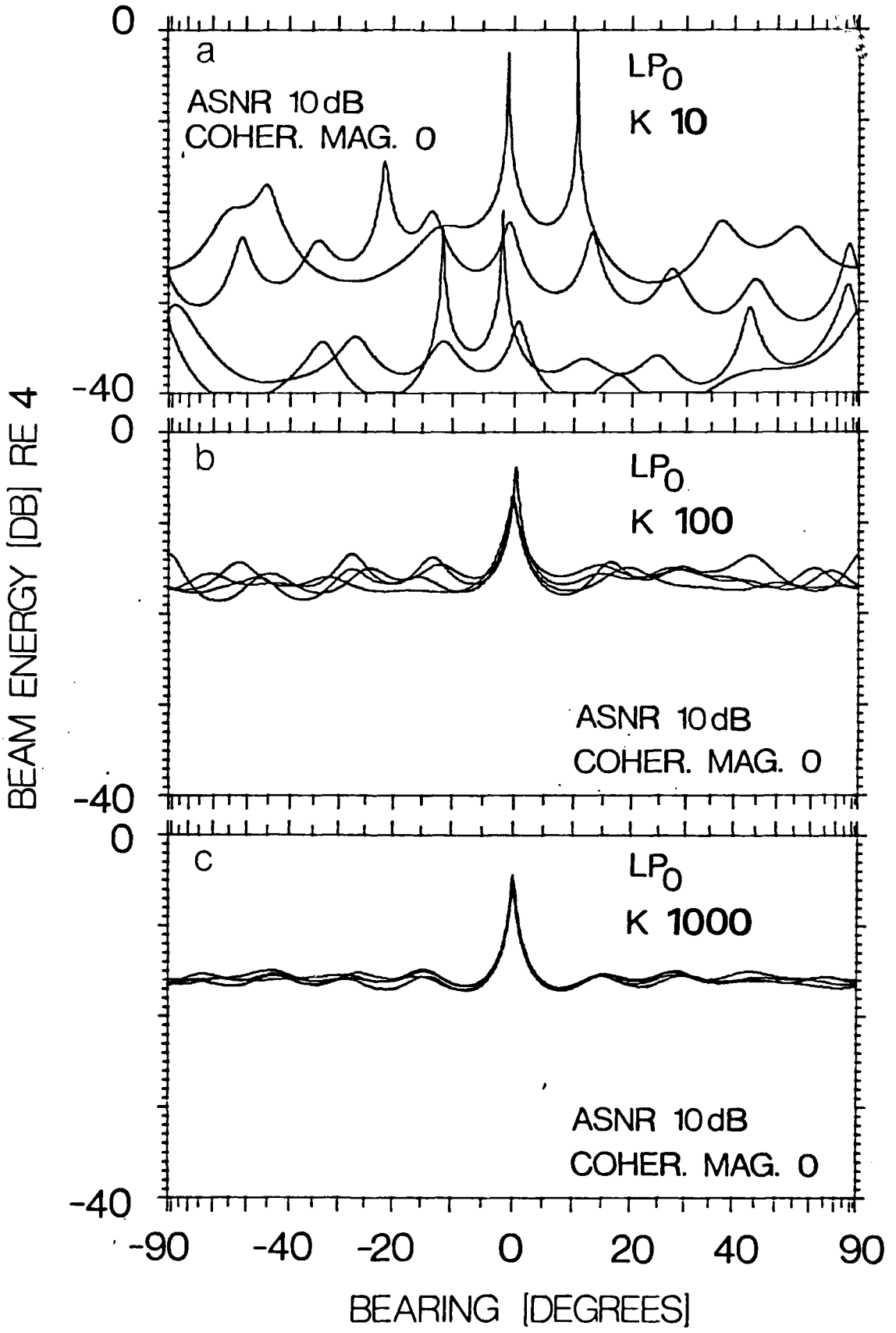
0
a
ASNR 10dB
COHER. MAG. 0
LP0
K 10
-40
0
b
LP0
K 100
ASNR 10dB
COHER. MAG. 0
-40
0
c
LP0
K 1000
ASNR 10dB
COHER. MAG. 0
-40
-90
-40
-20
0
20
40
90
BEAM ENERGY [DB] RE 4
BEARING [DEGREES]

FIGURE 14

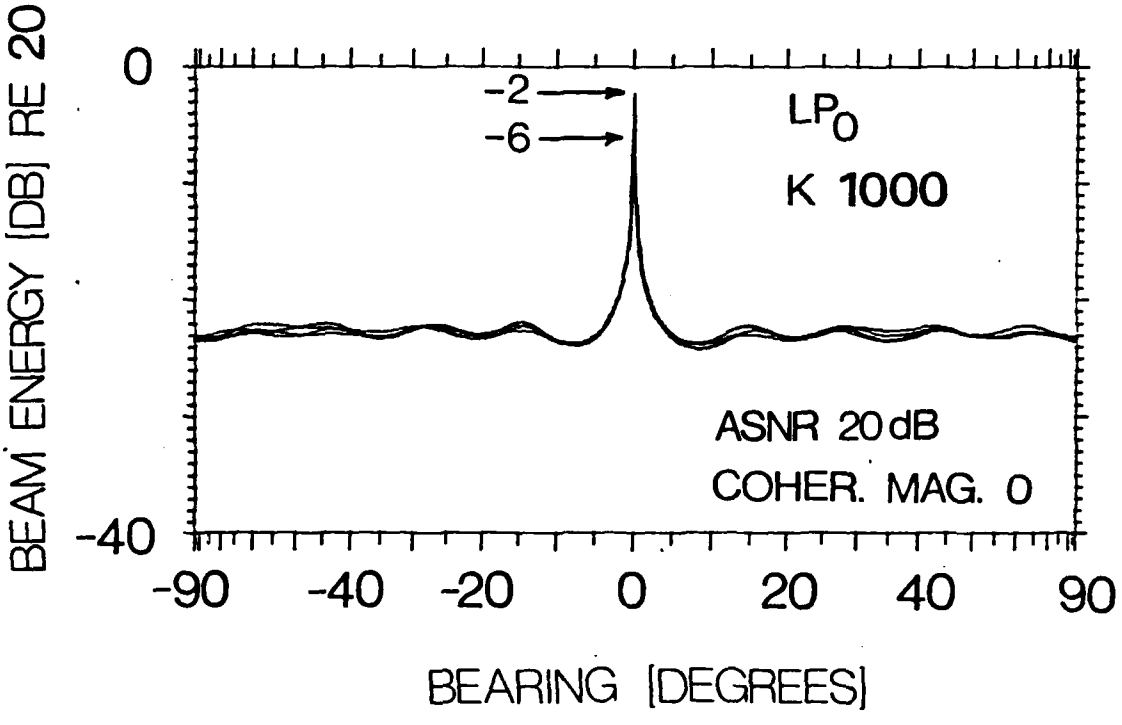
BEAM ENERGY [DB] RE 20
0
-40
-2
-6
LP0
K 1000
ASNR 20 dB
COHER. MAG. 0
-90
-40
-20
0
20
40
90
BEARING [DEGREES]

FIGURE 15

SECURITY CLASSIFICATION OF THIS PAGE (When Data Entered)

REPORT DOCUMENTATION PAGE		READ INSTRUCTIONS BEFORE COMPLETING FORM
1. REPORT NUMBER 8218	2. GOVT ACCESSION NO. A124 854	3. RECIPIENT'S CATALOG NUMBER
4. TITLE (and Subtitle) CAPABILITY OF ARRAY PROCESSING ALGORITHMS TO ESTIMATE SOURCE BEARINGS		5. TYPE OF REPORT & PERIOD COVERED TECHNICAL 6. PERFORMING ORG. REPORT NUMBER
7. AUTHOR(s) STUART R. DEGRAAF, DON H. JOHNSON		8. CONTRACT OR GRANT NUMBER(s) N00014-81-K-0565
9. PERFORMING ORGANIZATION NAME AND ADDRESS RICE UNIVERSITY P. O. BOX 1892 HOUSTON, TX 77251		10. PROGRAM ELEMENT, PROJECT, TASK AREA & WORK UNIT NUMBERS
11. CONTROLLING OFFICE NAME AND ADDRESS OFFICE OF NAVAL RESEARCH ARLINGTON, VA 22217 —		12. REPORT DATE DECEMBER 1982 13. NUMBER OF PAGES 36
14. MONITORING AGENCY NAME & ADDRESS(if different from Controlling Office)		15. SECURITY CLASS. (of this report) UNCLASSIFIED 15a. DECLASSIFICATION/ DOWNGRADING SCHEDULE

16. DISTRIBUTION STATEMENT (of this Report)

APPROVED FOR PUBLIC RELEASE: DISTRIBUTION UNLIMITED.

17. DISTRIBUTION STATEMENT (of the abstract entered in Block 20, if different from Report)

18. SUPPLEMENTARY NOTES

19. KEY WORDS (Continue on reverse side if necessary and identify by block number)

Array processing; beamforming; bearing estimation; bearing bias.

20. ABSTRACT (Continue on reverse side if necessary and identify by block number)

The capabilities of classical, minimum energy, and linear predictive array processing algorithms to estimate the bearings of two equal-energy sources is examined. Signal coherence is shown to affect adversely the resolution and detection capabilities, as well as the bias characteristics, of all three algorithms. For linear arrays of equally spaced sensors, the superior resolution capability of the linear predictive algorithm is demonstrated. The value of utilizing prediction elements in the center of the array to resolve very closely spaced source bearings is demonstrated. However, the

DD FORM 1 JAN 73 1473 EDITION OF 1 NOV 65 IS OBSOLETE
S N 0102-LF-014-6601

UNCLASSIFIED
SECURITY CLASSIFICATION OF THIS PAGE (When Data Entered)

linear predictive algorithm is least capable of detecting highly coherent sources. A tradeoff is established between resolving capability and sensitivity to finite averaging. Conditions are established which indicate which algorithm is best suited to anticipated levels of signal coherence and averaging. The estimates of source bearing produced by each algorithm are shown to be asymptotically biased. The bias produced by the classical beamformer is most severe, while the minimum energy beamformer produces the least bias.